Search for new charmed strange states in the $\Upsilon(2S)$ decay and e^+e^- annihilation

Baosheng Gao[1], XiaoLong Wang[2] and Minggang Zhao[1]

[1] *School of Physics, Nankai University, Tianjin, 300071, China and*

[2] *Institute of Modern Physics, Fudan University, Shanghai, 200433, China*

(Dated: May 29, 2025)

Abstract

We search for new charmed strange states in the process $\Upsilon(2S) \to D_s^{(*)+} D_{sJ}^-$ and in continuum production $e^+e^- \to D_s^{(*)+} D_{sJ}^-$ at $\sqrt{s} = 10.58$ GeV (and their charge conjugates), where D_{sJ}^- represents either $D_{s1}^*(2700)^-$ or $D_{s1}^*(2860)^-$. This analysis utilizes 158 ± 4 million $\Upsilon(2S)$ events and 89.5 fb^{-1} of continuum data samples collected at $\sqrt{s} = 10.58$ GeV. The Belle samples are converted into Belle II data format using B2BII in release-08-02-02. The D_J^- states under investigation are $D_{s1}^*(2700)^-$ or $D_{s1}^*(2860)^-$, identified through their decay into $\bar{D}^{(*)}\bar{K}$. Clear signals of $D_{s1}^*(2700)^-$ and $D_{s1}^*(2860)^-$ are observed in the $\Upsilon(2S)$ and continuum MC simulations. The mass resolutions are approximately 7.0 MeV/c^2 for $D_{s1}^*(2700)^-$ and 10.0 MeV/c^2 for $D_{s1}^*(2860)^-$. Results from the Belle data samples will be provided after the box opening.

PACS numbers: 14.40.Gx, 13.25.Gv, 13.66.Bc

CONTENTS

I. INTRODUCTION

Open charmed mesons, which consist of a charm quark and either an up, down, or strange quark, are crucial for testing quark model predictions within the Standard Model. Since their initial observation [1], numerous states have been identified [2]; however, the total still falls significantly short of the predictions made by conventional models [3, 4]. The search for excited open charmed mesons, denoted as $D_{(s)J}$, employs two primary methods: inclusive reactions and amplitude analyses of exclusive B meson decays. In the $c\bar{u}$ sector, states such as $D_J(2550)^0$, $D_J(2600)^0$, and $D_J(2750)^0$ have been observed by BaBar during the process $e^+e^- \to c\bar{c} \to D^{(*)}\pi X$ (where X represents any additional system) [5]. Their quantum numbers are further analyzed by LHCb in the decay $B^- \to D^{*+}\pi^-\pi^-$ [6]. In the $c\bar{s}$ system, the narrow state $D_{s0}(2317)^+$ has been observed in inclusive $D_s^+\pi^0$ final states [7] and subsequently confirmed by Belle in the decay $B \to \bar{D}D_{s0}(2317)$ [8]. Additionally, the broad state $D_{s1}^*(2700)$ has been observed in the decay $B \to \bar{D}D^0K^+$ by Belle [9], and later confirmed by BaBar in the D^*K final state through inclusive e^+e^- interactions. Meanwhile, BaBar has also provided the ratio of $D_{s1}^*(2700) \to KD^*/D_{s1}^*(2700) \to KD$ [10]. Recently, Belle has observed the process $\psi(2S) \to D_s^{*+}D_{sJ}$ and continuum production $e^+e^- \to D_s^{*+}D_{sJ}$ at $\sqrt{s} = 10.52$ GeV using innovative partial reconstruction techniques [11]. This novel approach offers a unique framework for the exploration of new charmed strange states.

This study focuses on the search for new charmed states in $D_s^{(*)+}D_{sJ}^-$ final states from $\Upsilon(2S)$ decays and e^+e^- annihilation, utilizing an innovative partial reconstruction technique. This approach promises to enhance our understanding of the production and annihilation mechanisms of charmed strange states.

II. ANALYSIS METHOD

We search for the $D_s^{(*)+}D_{sJ}^-$ final states with the subsequent decay $D_{sJ}^- \to \bar{D}^{(*)}\bar{K}$ in the $\Upsilon(2S)$ decays and the production of e^+e^- annihilation. We use the technique of partial reconstruction for the D_{sJ}^- final state, which is tagged through the recoil mass of the fully reconstructed $D_s^{(*)+}$, and the recoiling D_{sJ}^- is tagged by a kaon produced in the decay $D_{sJ}^- \to \bar{D}^{(*)}\bar{K}$. The remaining $\bar{D}^{(*)}$ is observed indirectly though its recoil against the $\bar{D}^{(*)}\bar{K}$ system using the known kinematics of the initial state. The circumvents the problem of low efficiencies for reconstructing $\bar{D}^{(*)}$ mesons associated with the large variety of possible decay processes.

III. DATA SAMPLES AND MC SIMULATION

This work is performed on the software frameworks of B2BII for the Belle analysis. The data samples for the analysis are:

- The Belle $\Upsilon(2S)$ data sample includes 24.7 fb^{-1} of data collected on the resonance and 1.7 fb^{-1} of off-resonance (continuum) data at $\sqrt{s} = 9.993$ GeV, along with a small scan data sample with a size of 258 pb^{-1}.

- The 89.5 fb^{-1} continuum data sample collected at $\sqrt{s} = 10.52$ GeV.

By measuring the inclusive hadronic decays, the number of $\Upsilon(2S)$ events produced is estimated to be $158 \pm 4 \times 10^6$ [12]. The 1.7 fb^{-1} off-resonance data sample is insufficient for studying backgrounds from QED continuum production; thus, the large continuum sample at $\sqrt{s} = 10.52$ GeV with an integrated luminosity of 89.5 fb^{-1} is utilized. For this analysis, the skim samples of HadronB(J) [13] and tau_skimB [14] are combined, with each event included in both samples counted only once. The efficiency of the combined skim selections is found to exceed 98%.

We utilize the EvtGen generator [15] to simulate the process $\Upsilon(2S)/e^+e^- \to D^{*+}D_J$ in accordance with the quantum numbers J^P of $D_s^{(*)+}$ and D_{sJ}^- [16]. Four decay modes of D_{sJ}^- are simulated: D^0K^-, $D^-K_S^0$, $D^*(2007)^0K^-$, and $D^*(2010)^+K_S^0$. The $\bar{D}^{(*)}$ meson is not reconstructed but is determined from the recoil against the $D_s^{(*)+}$ and kaon that decay from D_{sJ}^-, ensuring that the decay of $\bar{D}^{(*)}$ is treated inclusively. In this work, GEANT3 [17] is employed to simulate the detector responses, with the sizes of the generic MC samples corresponding to three times the integrated luminosity of the Belle data used to study the backgrounds.

IV. EVENT SELECTION AND RECONSTRUCTION

We search for the tagged D_s^+ using six final states: $\phi\pi^+$, $K_S^0K^+$, $\bar{K}^*(892)^0K^+$, $\rho^+\phi$, $\eta\pi^+$, and $\eta'\pi^+$, with the decay of the D_s^{*+} proceeding through $D_s^{*+} \to D_s^+\gamma$.

In this section, we present some selection criteria, distributions from MC simulations and data samples, as well as an analysis of the generic MC samples.

A. General selection

The following general selection criteria are applied to both the data samples and the MC simulations.

1. For a well-measured charged track, selection criteria are applied based on the parameters perpendicular to and along the beam direction with respect to the interaction point: $dr < 0.5$ cm and $|dz| < 2.0$ cm, respectively. The transverse momentum is required to be greater than 0.1 GeV/c in the lab frame. To identify a charged track (PID), information from different sub-detector systems is combined to form a likelihood for each particle species (i), denoted as $\mathcal{L}_i$. A well-measured charged track with $\mathcal{R}_K = \frac{\mathcal{L}_K}{\mathcal{L}_K+\mathcal{L}_\pi} < 0.4$ is identified as a pion candidate, while a track with $\mathcal{R}_K > 0.6$ is identified as a charged kaon candidate.

2. For K_S^0 candidates, a multivariate analysis using a neural network [18] is employed, based on two sets of input variables [19]. A K_S^0 candidate is constructed from a pair of oppositely charged tracks treated as pions.

3. An ECL cluster is considered a photon candidate if it does not match the extrapolation of any charged track. Pairs of photons are combined to form π^0 candidates. The energies of photons from π^0 decay are required to be greater than 25 MeV in the calorimeter barrel and 50 MeV in the calorimeter end caps in the laboratory frame. The η candidates are reconstructed via the $\gamma\gamma$ and $\pi^+\pi^-\pi^0$ decay modes. Photon candidates from $\eta \to \gamma\gamma$ are required to have energies exceeding 150 MeV in the laboratory frame. The reconstructed η candidates are combined with $\pi^+\pi^-$ pairs to form η' candidates. Mass and vertex constraint fits are applied to the π^0, η, and η' candidates.

4. The ϕ, $\bar{K}^*(892)^0$, and ρ^+ candidates are reconstructed in the K^+K^-, $K^-\pi^+$, and $\pi^0\pi^+$ decay modes. The mass windows applied for ϕ, $\bar{K}^*(892)^0$, ρ^+, π^0, $\eta \to \gamma\gamma$, $\eta \to \pi^+\pi^-\pi^0$, and η' candidates are detailed in Table I.

TABLE I. The mass window cuts for the selected meson candidates are set to approximately 3.0σ regions around the corresponding nominal mass of each meson.

Candidates	Mass window cut (MeV/c^2)
$\phi \to K^+K^-$	± 10
$K_S^0 \to \pi^+\pi^-$	± 15
$K^*(892)^0 \to K^+\pi^-$	± 105
$\pi^0 \to \gamma\gamma$	± 15
$\rho^+ \to \pi^0\pi^+$	± 200
$\eta \to \gamma\gamma$	± 40
$\eta \to \pi^+\pi^-\pi^0$	± 12
$\eta' \to \pi^+\pi^-\eta$	± 15

B. Reconstruction of D_s^+ and D_s^{*+}

Before calculating the mass of the D_s^+ candidates, a fit to a common vertex is performed for the charged tracks within the D_s^+ candidates. Figs. 1 display the combined distribution $M_{\mathrm{h_1h_2}}$ for $M_{\phi\pi^+}$, $M_{K_S^0K^+}$, $M_{\bar{K}^*(892)^0K^+}$, $M_{\rho^+\phi}$, $M_{\eta\pi^+}$, and $M_{\eta'\pi^+}$ for the D_s^+ candidates. These figures are derived from the data samples and signal MC simulations. The D_s^+ signal is fitted using a double Gaussian function, while the background is described by a first-order (or second-order) polynomial function. In this context, we define the mass resolution of the D_s^+ signals using the formula $\sigma \equiv \sqrt{f_1 \times (\sigma_1^2 + m_1^2) + f_2 \times (\sigma_2^2 + m_2^2) - m^2}$ with $m = f_1 \times m_1 + f_2 \times m_2$, where m_1 (m_2), σ_1 (σ_2), and f_1 (f_2) represent the mean, standard deviation, and fraction of the second Gaussian function, respectively. A mass resolution of $\sigma_{D_s^+} = 8.3 \pm 0.9$ MeV/c^2 is obtained from the data, which is used to define the signal region for D_s^+, while the corresponding resolution in signal MC simulations is 8.7 MeV/c^2. Additionally, we define sideband regions using the criterion $|M_{h_1h_2} - m_{D_s^+} \pm 9\sigma_{D_s^+}| < 3\sigma_{D_s^+}$, which is twice as wide as the signal region. Since the fraction of multi-combination in D_s^+ reconstruction is approximately 3%, multiple D_s^+ candidates are allowed in a single event.

We reconstruct D_s^{*+} candidates from the D_s^+ sample using the γD_s^+ final state. For this, we require the photon energy to exceed $E_\gamma > 50$ MeV in the barrel and $E_\gamma > 100$ MeV in the endcaps of the ECL. The corresponding invariant mass distributions $M_{\gamma D_s^+}$ for γD_s^+ from

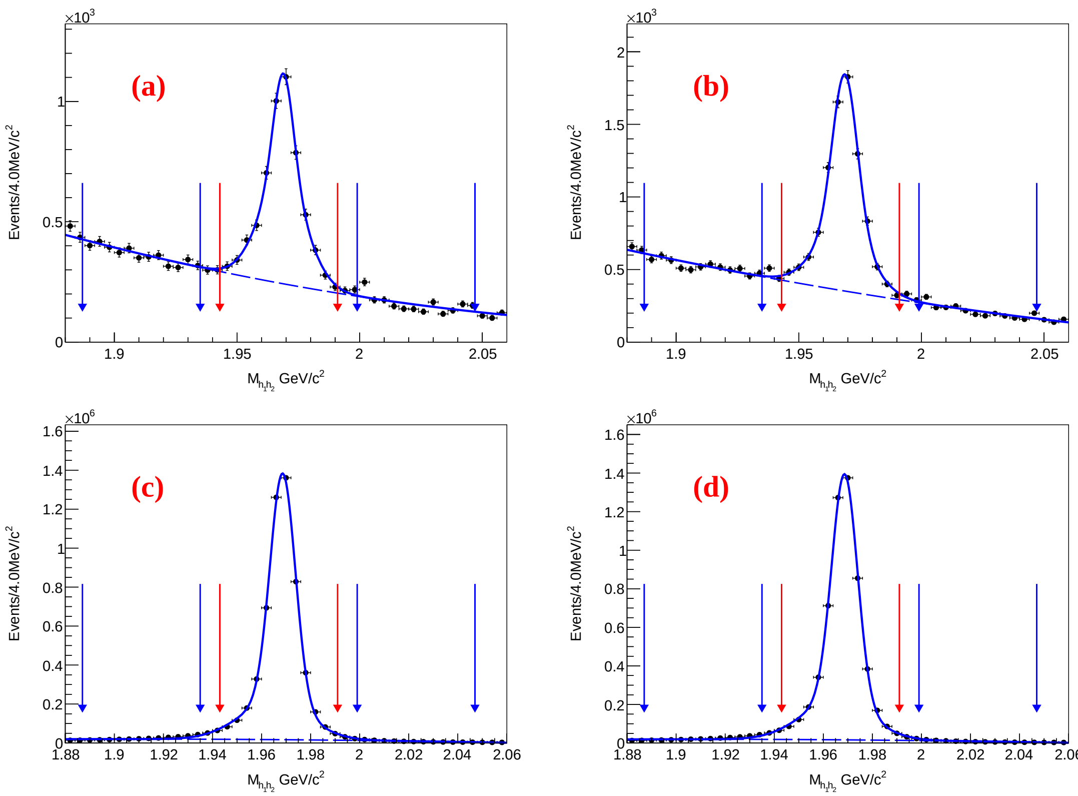

FIG. 1. Invariant mass distributions of the combinations of $\phi\pi^+$, $K_S^0K^+$, $\bar{K}^*(892)^0K^+$, $\rho^+\phi$, $\eta\pi^+$, and $\eta'\pi^+$ for the D_s^+ candidates are presented in the following: (a) the $\Upsilon(2S)$ data samples, (b) the continuum data sample at $\sqrt{s} = 10.58$ GeV, (c) the signal MC simulations of $\Upsilon(2S)$ decays, and (d) the signal MC simulation of continuum production at $\sqrt{s} = 10.58$ GeV. The red arrows show the signal region of D_s^+, and the blue arrows show the related sideband regions. The curves show the best fit results using Gaussian functions for the D_s^+ signals.

the $\Upsilon(2S)$ and continuum data samples are shown in Fig. 2. We fit the $M_{\gamma D_s^+}$ distribution between 2.07 GeV/c^2 and 2.15 GeV/c^2 using two Gaussian functions for the D_s^{*+} signal and a second-order polynomial function for the background. We obtain a mass resolution of $\sigma_{D_s^{*+}} = 8.2 \pm 0.4$ MeV/c^2 in data and 6.0 MeV/c^2 in signal MC simulations, which agree well with each other. In addition to defining the signal region for D_s^{*+}, we also establish sideband regions using the criterion $|M_{\gamma D_s^+} - m_{D_s^{*+}} \pm 9\sigma_{D_s^{*+}}| < 3\sigma_{D_s^{*+}}$.

As we aim to study the $D_s^{*+}\bar{K}$ recoil spectrum, we apply mass-constrained fits to the D_s^{*+} candidates in the signal region to improve their momentum resolution. We find that 11% of the events have multiple D_s^{*+} candidates. In these cases, we select the candidate with the minimum χ^2 from the mass-constraint fit. For candidates in each D_s^{*+} mass sideband,

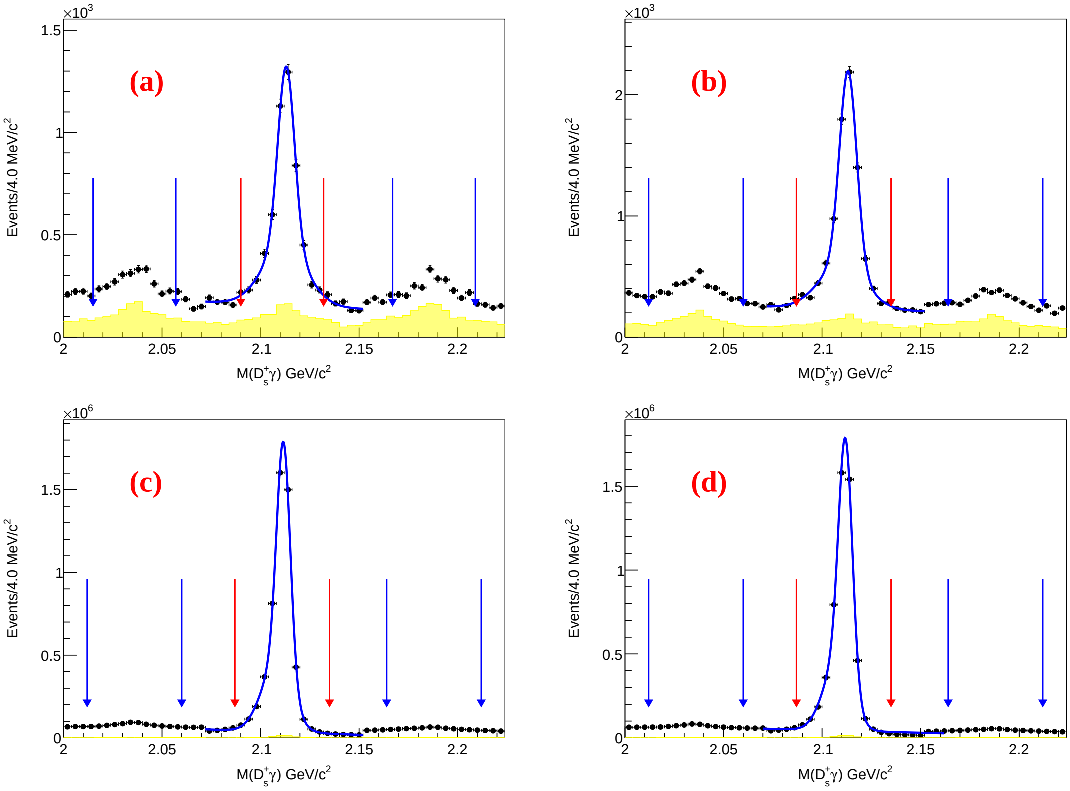

FIG. 2. Invariant mass distributions of the combination of $D_s^+\gamma$ for the D_s^{*+} candidates are presented in the following: (a) the $\Upsilon(2S)$ data samples, (b) the continuum data sample at $\sqrt{s} =$ 10.58 GeV, (c) the signal MC simulations of $\Upsilon(2S)$ decays, and (d) the signal MC simulation of continuum production at $\sqrt{s} = 10.58$ GeV. The red arrows show the signal region of D_s^+ or $D_s^{(*)+}$, and the blue arrows show the related sideband regions. The shaded histograms illustrate the backgrounds estimated from the normalized D_s^+ mass sidebands. The curves show the best fit results using Gaussian functions for the D_s^{*+} signals.

we apply the mass constraint to the center of the sideband and select the combination with the minimum χ^2 as well. To estimate the size of the peaking component in the selected D_s^{*+} sample due to the minimum χ^2 requirement, we apply the same mass constraints to events in the D_s^+ sidebands. As shown in Fig. 2, the D_s^+ mass sideband events can effectively describe the peaks in the D_s^{*+} mass sidebands and therefore can be used to reliably estimate the peaking component in the D_s^{*+} mass signal region. Events with $|M_{\gamma D_s^+} - m_{D_s^{*+}}| < 3\sigma_{D_s^{*+}}$ are removed for the $D_s^+ D_{sJ}^-$ search.

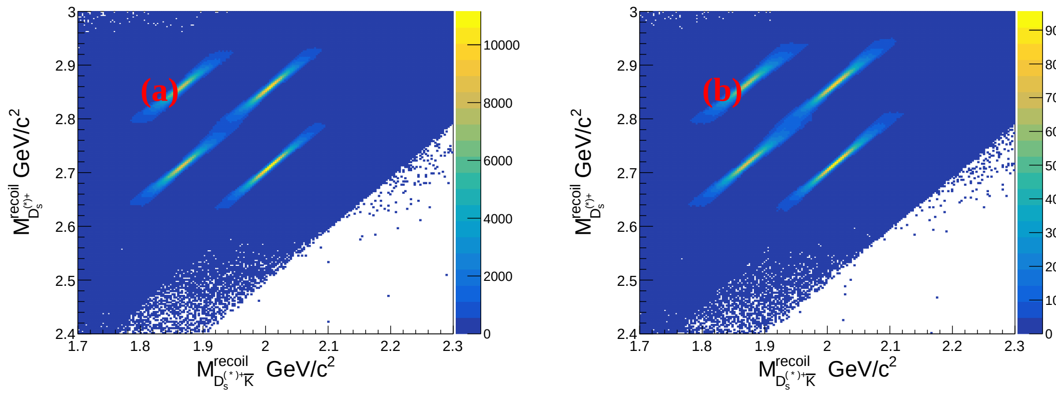

FIG. 3. The distributions of the recoil mass against $D_s^{(*)+}\bar{K}$ versus the recoil mass against $D_s^{(*)+}$ (a) the signal MC simulation of $\Upsilon(2S)$ decays and (b) the signal MC simulation of continuum production at $\sqrt{s} = 10.52$ GeV.

C. The study of recoil mass spectra against the $D_s^{(*)+}\bar{K}$ in the $\Upsilon(2S)$ and continuum at $\sqrt{s} = 10.52$ GeV signal MC simulations

The search for $\bar{D}^{(*)}$ requires the reconstruction of a $\bar{K}$ meson in addition to the $D_s^{(*)+}$. We determine the $\bar{D}^{(*)}$ signal through the recoil of $D_s^{(*)+}\bar{K}$ using the calculated mass:

$$M_{\bar{D}^{(*)}} = M^{\rm recoil}_{D_s^{(*)+}\bar{K}} \equiv \sqrt{(E_{\rm c.m.} - E_{D_s^{(*)+}} - E_{\bar{K}})^2 - (\vec{p}_{\rm c.m.} - \vec{p}_{D_s^{(*)+}} - \vec{p}_{\bar{K}})^2}, \quad (1)$$

and isolate the possible production of D_{sJ}^- states in the $\bar{K}\bar{D}^{(*)}$ final states through their recoil using the following equation:

$$M_{\bar{K}\bar{D}^{(*)}} = M^{\rm recoil}_{D_s^{(*)+}} \equiv \sqrt{(E_{\rm c.m.} - E_{D_s^{(*)+}})^2 - (\vec{p}_{\rm c.m.} - \vec{p}_{D_s^{(*)+}})^2}. \quad (2)$$

Here, $E_{\rm c.m.}$ and $\vec{p}_{\rm c.m.}$ denote the energy and 3-momentum of the e^+e^- collision system, while $E_{D_s^{(*)+}}$ ($E_{\bar{K}}$) and $\vec{p}_{D_s^{(*)+}}$ ($\vec{p}_{\bar{K}}$) correspond to those of $D_s^{(*)+}$ ($\bar{K}$), respectively.

We present the distributions of $M^{\rm recoil}_{D_s^{(*)+}\bar{K}}$ versus $M^{\rm recoil}_{D_s^{(*)+}}$ from the two signal MC simulations of $\Upsilon(2S)$ decays and continuum production in Fig. 3(a) and (b), respectively. Clear bands are observed in the MC simulation distributions, corresponding to the production of the $D_{s1}^*(2700)^-$ or $D_{s1}^*(2860)^-$ signal in the $\bar{D}^*\bar{K}$ ($\bar{D}^*(2007)^0K^-$ or $D^*(2010)^-K_S^0$) final state, and the $D_{s2}(2573)^-$ or $D_{s1}^*(2700)^-$ signal in the $\bar{D}^0\bar{K}$ ($\bar{D}^0K^-$ or $D^-K_S^0$) final state.

The mass resolutions of $M^{\rm recoil}_{D_s^{(*)+}\bar{K}}$ and $M^{\rm recoil}_{D_s^{(*)+}}$ are relatively large due to the common variables $E_{D_s^{(*)+}}$ and $\vec{p}_{D_s^{(*)+}}$ in Eqs. (1) and (2). To improve the mass resolution of $M_{\bar{K}\bar{D}^{(*)}}$,

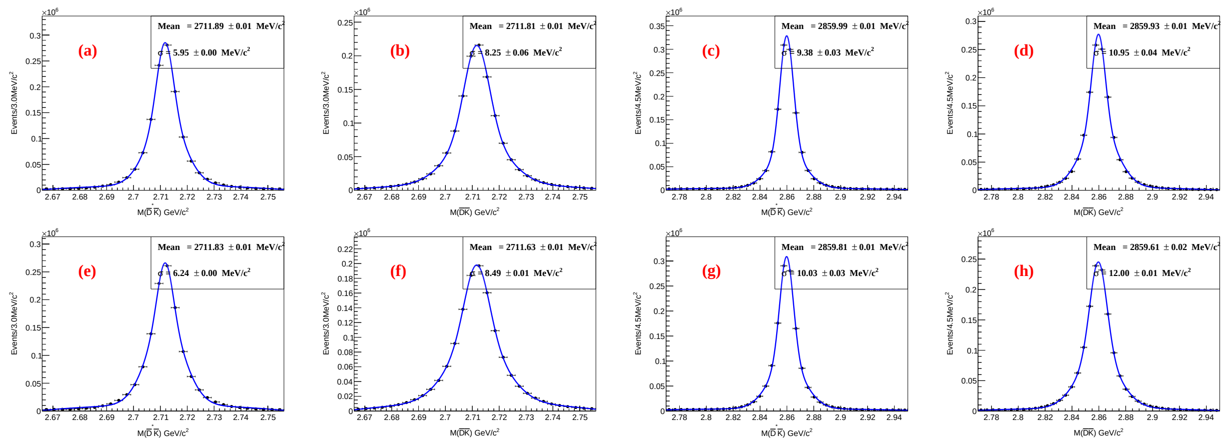

FIG. 4. The invariant mass distributions of $\bar{K}\bar{D}^*$ calculated in the recoil mass for $D_s^{(*)+}$ are presented for the following decay modes: (a) $D_{s1}^*(2700)^- \to \bar{D}^*\bar{K}$, (b) $D_{s1}^*(2700)^- \to \bar{D}\bar{K}$, (c) $D_{s1}^*(2860)^- \to \bar{D}^*\bar{K}$, and (d) $D_{s1}^*(2860)^- \to \bar{D}\bar{K}$. These distributions are obtained from the $\Upsilon(2S)$ signal MC simulations (top panels) and the continuum signal MC simulations at 10.52 GeV (bottom panels) as shown in (e)-(h). The curves show the best fit results using Gaussian functions for the D_s^+ signals.

we employ the following formula to replace Eq. (2):

$$M_{\bar{K}\bar{D}^{(*)}} = M^{\text{recoil}}_{D_s^{(*)+}} - M^{\text{recoil}}_{D_s^{(*)+}\bar{K}} + m_{\bar{D}^{(*)}}. \tag{3}$$

This adjustment significantly reduces the uncertainties arising from the 4-momentum of final states from $D_s^{(*)+}$ decays. From simulation, Fig. 3 shows the distributions of $M(\bar{K}\bar{D}^{(*)})$ for all $D_s^{(*)+}D_{sJ}^-$ final states. From these distributions, we obtain resolutions of $\sigma_{\bar{K}\bar{D}^{(*)}} <$ 10 MeV/c^2.

V. BACKGROUND STUDY

The background study presented in this research primarily underscores the analysis of Generic MC distributions and the execution of cross-feeding checks.

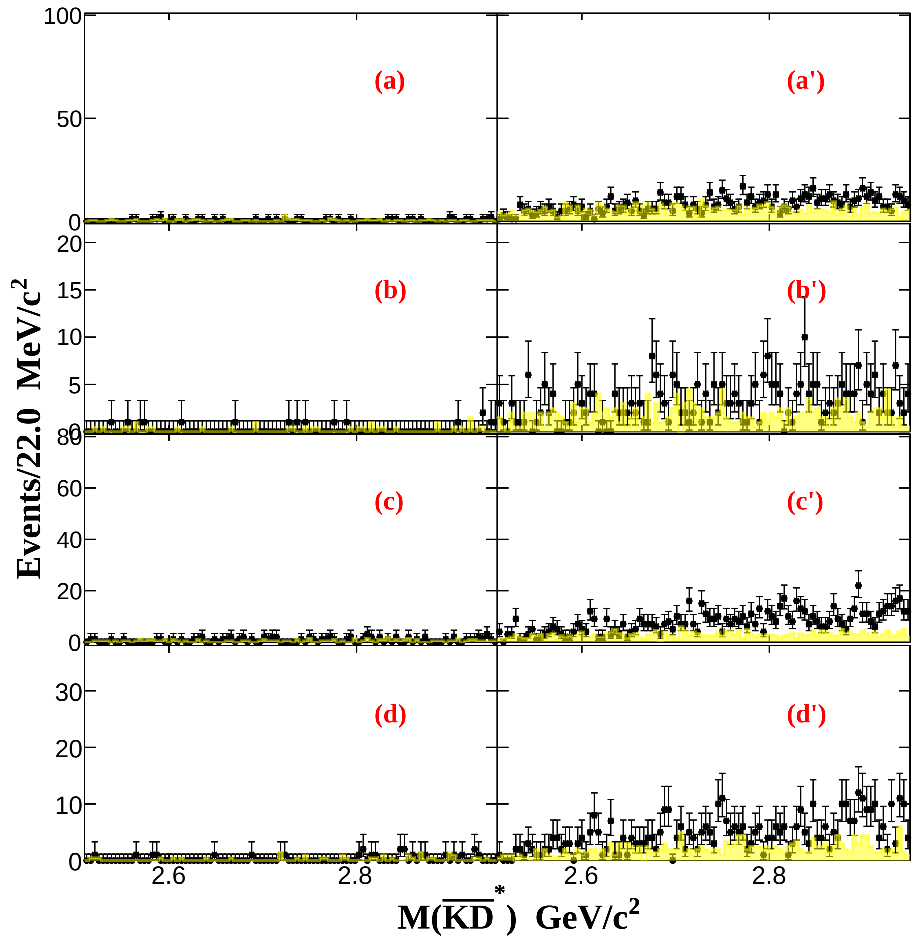

FIG. 5. The invariant mass distributions of $\bar{K}\bar{D}^*$ calculated in the recoil mass for $D_s^{(*)+}$ in the (a) $D_s^+ K^- \bar{D}^*(2007)^0$, (b) $D_s^+ K_S^0 D^*(2010)^+$, (c) $D_s^{*+} K^- \bar{D}^*(2007)^0$, and (d) $D_s^{*+} K_S^0 D^*(2010)^+$ final states from the $\Upsilon(2S)$ generic MC simulations (left panels) and the continuum generic MC simulations at 10.52 GeV (right panels). The shaded histograms show the backgrounds estimated from the normalized $D_s^{(*)+}$ mass sidebands.

A. Generic MC study

We use $e^+e^- \to q\bar{q}(u\bar{u},\, d\bar{d},\, s\bar{s},\, c\bar{c},\, b\bar{b})$ at $\sqrt{s} = 10.52\,\mathrm{GeV}/c^2$, with three times the luminosity of the real data, along with $\Upsilon(2S)$ generic MC samples on $\Upsilon(2S) \to q\bar{q}(u\bar{u},\, d\bar{d},\, s\bar{s},\, c\bar{c})$ containing 1×10^8 events to study the background. The distributions of $M(\bar{D}^{(*)}\bar{K})$ are shown in Fig. 5 and Fig. 6. From these distributions, we find that there are no peaking backgrounds.

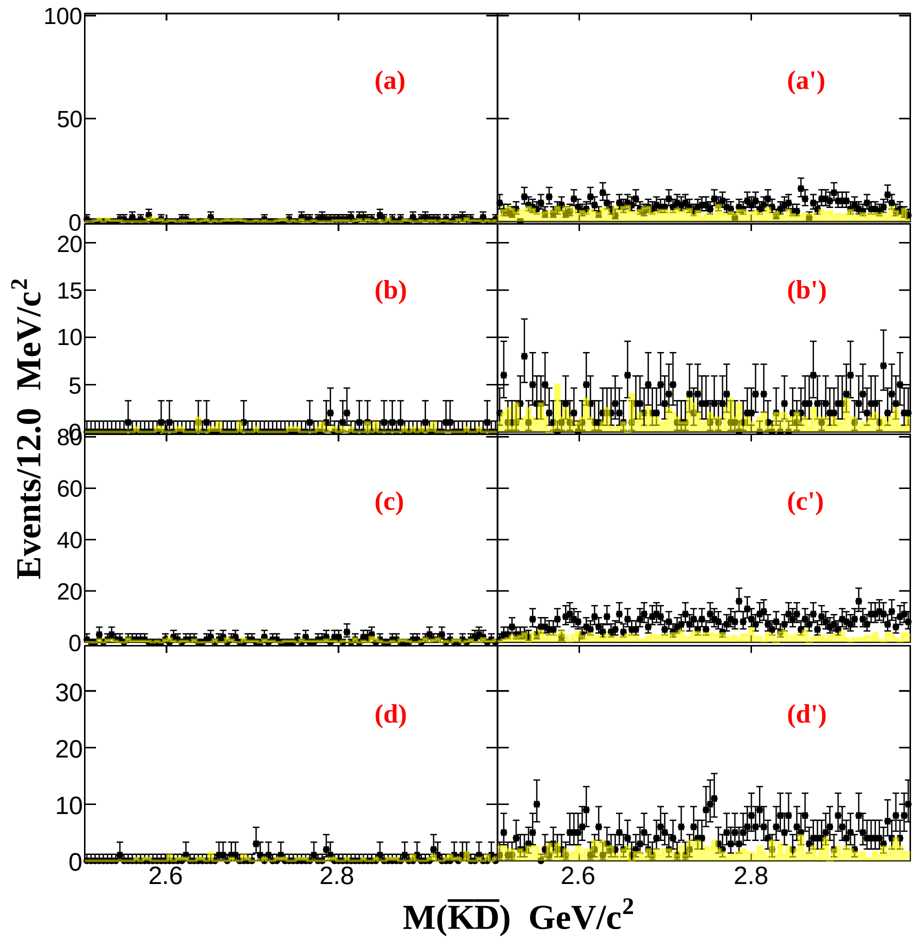

FIG. 6. The invariant mass distributions of $\bar{K}\bar{D}$ calculated in recoil mass for $D_s^{(*)+}$ in the (a) $D_s^+K^-\bar{D}^0$, (b) $D_s^+K_S^0D^-$, (c) $D_s^{*+}K^-\bar{D}^0$, and (d) $D_s^{*+}K_S^0D^-$ final states from the $\Upsilon(2S)$ generic MC simulations (left panels) and the continuum generic MC simulations at 10.52 GeV (right panels). The shaded histograms show the backgrounds estimated from the normalized $D_s^{(*)+}$ mass sidebands.

B. Cross-feeding checks

For the selection of the $\Upsilon(2S)/e^+e^- \to D_s^+D_{sJ}^-$ final states, the process $\Upsilon(2S)/e^+e^- \to D_s^{*+}D_{sJ}^-$ can also be considered a source of $\Upsilon(2S)/e^+e^- \to D_s^+D_{sJ}^-$ events when D_s^+ candidates are combined with a soft photon to form D_s^{*+} candidates. In this case, the condition $|M_{\gamma D_s^+} - m_{D_s^{*+}}| < 3\sigma_{D_s^{*+}}$ is applied, which leads to the rejection of some D_s^{*+} candidates. However, this approach results in a 30% reduction in efficiency. Consequently, the $D_s^{*+}D_{sJ}^-$ final states will not overlap with the candidate particles selected for the $D_s^+D_{sJ}^-$ event selec-

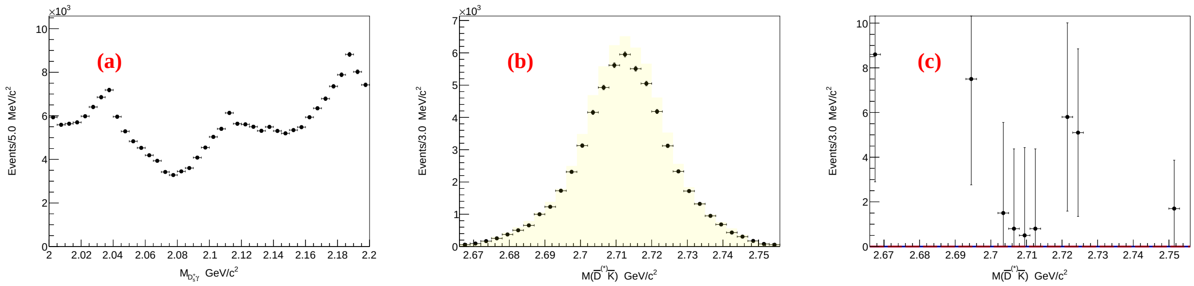

FIG. 7. The invariant mass distributions of (a)$D_s^+\gamma$, (b) and (c) are distributions of $M(\bar{D}^{(*)}\bar{K})$ before and after subtracting the background from the D_s^{*+} sidebands, respectively. The shaded histograms illustrate the backgrounds estimated from the normalized D_s^{*+} mass sidebands.

tions.

For the selection of the $D_s^{*+}D_{sJ}^-$ final states, the process $\Upsilon(2S)/e^+e^- \to D_s^+D_{sJ}^-$ can also be regarded as a source for $\Upsilon(2S)/e^+e^- \to D_s^{*+}D_{sJ}^-$. To investigate this situation, a signal MC simulations for $D_s^+D_{sJ}^-$ has been generated to cross-check the $D_s^{*+}D_{sJ}^-$ process. Fig. 7(a) shows the invariant mass distribution of $D_s^+\gamma$, while Fig. 7(b) and 7(c) present the distributions of $M(\bar{D}^{(*)}\bar{K})$ before and after the subtraction of the background from the D_s^{*+} sidebands, respectively. From these figures, it is clear that there is no cross-feeding between the $\Upsilon(2S)/e^+e^-D_s^+D_{sJ}^-$ and $\Upsilon(2S)/e^+e^-D_s^{*+}D_{sJ}^-$ processes.

VI. BORN CROSS SECTION AND BRANCHING FRACTION CALCULATION

We calculate the branching fraction of $\Upsilon(2S) \to D_s^{(*)+}D_{sJ}^-$ and the Born cross section for $e^+e^- \to D_s^{(*)+}D_{sJ}^-$ using the following equations:

$$\mathcal{B}(\Upsilon(2S) \to D_s^{(*)+}D_{sJ}^-)\mathcal{B}(D_{sJ}^- \to \bar{K}\bar{D}^{(*)}) = \frac{N_{\Upsilon(2S)}^{\rm sig}}{N_{\Upsilon(2S)} \times \sum \varepsilon_i \mathcal{B}_i}, \tag{4}$$

and

$$\sigma^{\rm B}(e^+e^- \to D_s^{(*)+}D_{sJ}^-)\mathcal{B}(D_{sJ}^- \to \bar{K}\bar{D}^{(*)}) = \frac{N_{\rm cont}^{\rm sig} \times |1-\Pi|^2}{\mathcal{L}_{\rm cont} \times \sum \varepsilon_i \mathcal{B}_i \times (1+\delta_{\rm ISR})}. \tag{5}$$

Here, i identifies the decay mode of the $D_s^+ \to h_1h_2$ decay, while ε_i and $\mathcal{B}_i$ represent their reconstruction efficiencies and branching fractions, respectively. We calculate $\sum \varepsilon_i \mathcal{B}_i$ based on signal MC simulations for ε_i and the world average values of $\mathcal{B}_i$ [2], with the results listed in Table II. Additionally, we account for the branching fraction of the $K_S^0 \to \pi^+\pi^-$ decay [2].

From the Born cross sections, we determine the full ”dressed” cross section using the formula $\sigma^{\rm dressed} = \sigma^{\rm Born}/|1-\Pi|^2$. The factor $|1-\Pi|^2 = 0.931$ denotes the vacuum polarization factor [20, 21]. Furthermore, we correct for radiative effects. The radiative correction factor $1+\delta_{\rm ISR}$ is obtained from the integral $\int \sigma^{\rm dressed}(s(1-x))F(x,s)\,dx/\sigma^{\rm dressed}(s)$ and has a value of 0.82, where $F(x,s)$ is the radiative function derived from a QED calculation with an accuracy of 0.2% [22–24].

To assess the reliability of this work, we compare our results with those from Belle [11], as detailed in Sec. IX. The comparison reveals that our results are in strong agreement with those from Belle.

TABLE II. The $\sum \varepsilon_i \mathcal{B}_i$ denotes the sum of the products of the reconstruction efficiencies and branching fractions across the six decay channels of D_s^+ for the study of $\Upsilon(2S)/e^+e^- \to D_s^{(*)+} D_{sJ}^- +$ *c.c.* In the case of the K_S^0 mode, $\sum \varepsilon_i \mathcal{B}_i$ is multiplied by the branching ratio for $K_S^0 \to \pi^-\pi^+$.

Final states	$\sum \varepsilon_i \mathcal{B}_i$			
	continuum MC simulations		$\Upsilon(2S)$ MC simulations	
	K^- mode (%)	K_S^0 mode (%)	K^- mode (%)	K_S^0 mode (%)
$D_s^+ D_{s1}^*(2700)^-(\to \bar{D}^* \bar{K})$	1.76 ± 0.03	1.07 ± 0.02	1.72 ± 0.02	1.05 ± 0.02
$D_s^{*+} D_{s1}^*(2700)^-(\to \bar{D}^* \bar{K})$	1.54 ± 0.02	0.89 ± 0.01	1.55 ± 0.02	0.89 ± 0.01
$D_s^+ D_{s1}^*(2700)^-(\to \bar{D} \bar{K})$	1.42 ± 0.02	0.88 ± 0.01	1.37 ± 0.02	0.87 ± 0.01
$D_s^{*+} D_{s1}^*(2700)^-(\to \bar{D} \bar{K})$	1.19 ± 0.23	0.74 ± 0.01	1.19 ± 0.02	0.73 ± 0.01
$D_s^+ D_{s1}^*(2860)^-(\to \bar{D}^* \bar{K})$	1.84 ± 0.03	1.11 ± 0.02	1.90 ± 0.03	1.16 ± 0.02
$D_s^{*+} D_{s1}^*(2860)^-(\to \bar{D}^* \bar{K})$	1.56 ± 0.02	0.91 ± 0.01	1.60 ± 0.02	0.94 ± 0.01
$D_s^+ D_{s1}^*(2860)^-(\to \bar{D} \bar{K})$	1.53 ± 0.02	0.97 ± 0.01	1.60 ± 0.02	1.00 ± 0.01
$D_s^{*+} D_{s1}^*(2860)^-(\to \bar{D} \bar{K})$	1.26 ± 0.02	0.78 ± 0.01	1.31 ± 0.02	0.81 ± 0.01

VII. SYSTEMATIC UNCERTAINTIES

Determining the branching fractions in $\Upsilon(2S)$ decays and the Born cross sections for continuum productions involves various systematic uncertainties. These include factors related to detection efficiency, such as tracking efficiency and particle identification, as well as uncertainties associated with the reconstruction of K_S^0 and π^0 mesons and the application of mass window cuts. Additionally, uncertainties in the branching fractions of intermediate states and in the angular distribution contribute to the overall systematic uncertainties, as outlined in Table III.

A. Detection Efficiency

1. Regarding tracking efficiency, recent updates estimate the efficiency for high-momentum tracks with $P_T > 200$ MeV$/c$ using partially reconstructed D^{*+} decays in $D^{*+} \to \pi^+ D^0$, $D^0 \to K_S^0\pi^+\pi^-$ [25]. A conservative estimation of the systematic uncertainty for high-momentum tracks is taken as 0.35% per track.

2. Regarding particle identification (PID), updated measurements of the particle identification efficiency using inclusive samples $D_s^{*+} \to \pi^+ D^0$ and $D^0 \to K^+\pi^-$ [26] indicate uncertainties of 1.1% for each kaon and 0.9% for each pion based on signal MC data simulations. Uncertainties from the same type of tracks are added linearly, while uncertainties from different types of tracks are summed in quadrature to obtain the final PID uncertainty.

3. Regarding K_S^0 selection, previous studies [27] have found the ratio of efficiencies in K_S^0 selection between data samples and MC simulations to be $(97.89 \pm 0.41 \pm 0.6)\%$. Thus, a systematic uncertainty of 2.23% is assigned for K_S^0 selection.

4. Regarding π^0 selection, the efficiency correction (0.957) and systematic uncertainty (2.25%) are determined from studying the control sample of $\tau^- \to \pi^-\pi^0\nu$ [28].

5. Regarding mass window cuts, the systematic uncertainties for ϕ, K_S^0, $K^*(892)^0$, π^0, ρ^+, $\eta(\to \gamma\gamma \,\text{or}\, \pi^+\pi^-\pi^0)$, η', D_s^+, and D_s^{*+} in the search for $\Upsilon(2S) \to D_s^{(*)+} D_{sJ}^- + c.c.$ with $D_{sJ}^- \to D^{(*)0} K^-$ and $D_{sJ}^- \to D^{(*)-} K_S^0$ are applied to estimate the uncertainties for both the signal MC simulation and data samples.

To summarize the systematic uncertainties related to detection efficiency for each final state, uncertainties from tracking efficiency, particle ID, K_S^0, and π^0 selection are first combined in quadrature to obtain σ_i (where i corresponds to different D_s^+ decay modes).

Next, to calculate the total detection-efficiency-related uncertainties (σ_{DER}) for the measurement of $\mathcal{B}[\Upsilon(2S) \rightarrow D_s^{(*)+} D_{sJ}^-]$, σ_{DER} is computed using the formula $\sigma_{DER} = \frac{\sqrt{\Sigma_i(\Delta\epsilon_i \times \mathcal{B}_i)}}{\Sigma_i(\epsilon_i \times \mathcal{B}_i)}$, where $\Delta\epsilon_i$ equals $\sigma_i \times \epsilon_i$, representing the absolute uncertainties of the efficiency for each D_s^+ decay mode.

B. Branching Fractions

In the calculations of branching fractions, the uncertainties of the branching fractions contribute to $\Sigma_i(\varepsilon_i \times \mathcal{B}_i)$. The uncertainties of the branching fractions, denoted as $\sigma_{\mathcal{B}}$, are calculated according to $\frac{\sqrt{\Sigma_i(\varepsilon_i \times \Delta\mathcal{B}_i)}}{\Sigma_i(\varepsilon_i \times \mathcal{B}_i)}$.

The total uncertainties $\Sigma\mathcal{B}_i$ represent the absolute uncertainties of the branching fractions for each of the D_s^+ decay modes, which are 0.06%, 0.06%, 0.06%, 0.17%, 0.05%, and 0.05% for $\phi\pi^+$, $K_S^0 K^+$, $K^*(892)^0 K^+$, $\phi\rho^+$, $\eta\pi^+$, and $\eta'\pi^+$, respectively [27]. The uncertainties in the branching fraction of D_s^{*+} for each of the D_s^+ decay modes are 0.06%, 0.06%, 0.06%, 0.26%, 0.05%, and 0.05%. We determine the total uncertainties of $\Sigma\varepsilon_i \times \mathcal{B}_i$ to be 2.2%, 2.2%, 2.4%, and 2.4% for the $D_s^+ K^- \bar{D}^{(*)}$, $D_s^+ K_S^0 \bar{D}^{(*)}$, $D_s^{*+} K^- \bar{D}^{(*)}$, and $D_s^{*+} K_S^0 \bar{D}^{(*)}$ final states, respectively.

C. Uncertainties in angular distribution

To estimate the systematic uncertainty in the angular distribution of $D_s^{(*)+}\pi^-$, we generate new MC simulations uniformly with phase space and take half of the efficiency difference as systematic uncertainties. The systematic uncertainties are 6.9%, 6.8%, 8.3%, and 9.5% for $D_s^+ K^- \bar{D}^{(*)0}$, $D_s^+ K_S^0 \bar{D}^{(*)-}$, $D_s^{*+} K^- \bar{D}^{(*)0}$, and $D_s^{*+} K_S^0 \bar{D}^{(*)-}$, respectively.

D. Interference between the resonance and continuum amplitudes in the $\Upsilon(2S)$ data

To be studied after the box opening.

E. Other uncertainties

The uncertainty in the total number of $\Upsilon(2S)$ events is 2.2%. The systematic uncertainties in the luminosities for the three data samples are 1.4%. By adjusting $S_{\rm cont}/S_{\Upsilon(2S)}$ to $[S_{\rm cont}/S_{\Upsilon(2S)}]^{1.5}$, the value of $f_{\rm scale}$ changes from 0.304 to 0.319, and we take 4.9% as its systematic uncertainty.

VIII. SUMMARY

For the first time, we employ a partial reconstruction technique to search for new charm-strange states in the decay $\Upsilon(2S)/e^+e^- \to D_s^{(*)+}D_{sJ}^-$ using data collected from approximately 158 ± 4 million $\Upsilon(2S)$ events and 89.5 fb^{-1} of continuum samples at $\sqrt{s} = 10.58$ GeV. The D_J^- states under investigation are $D_{s1}^*(2700)^-$ or $D_{s1}^*(2860)^-$, identified through their decays into $\bar{D}^{(*)}\bar{K}$. We fully reconstruct $D_s^{(*)+}K^-/K_S^0$, allowing the $\bar{D}^{(*)}$ to be missing to enhance efficiency. Clear signals for $D_{s1}^*(2700)^-$ and $D_{s1}^*(2860)^-$ are observed in both $\Upsilon(2S)$ and continuum MC simulations. No peaking backgrounds have been found in the generic MC samples, and cross-feeding checks indicate no overlap between the processes $\Upsilon(2S)/e^+e^- \to D_s^+D_{sJ}^-$ and $\Upsilon(2S)/e^+e^- \to D_s^{*+}D_{sJ}^-$. To further validate our works, we investigate the process $\Upsilon(2S)/e^+e^- \to D_s^{(*)+}D_{s1}(2536)^-/D_{s2}(2573)^- + c.c.$ and compare our results with those from Belle [11], which shows excellent agreement. Finally, we will present our results in the higher-mass region following the open box.

TABLE III. The summary of systematic uncertainties (%) of $D_s^{(*)+}K$ reconstruction. Additional uncertainties due to the angular distributions are 6.9%, 6.8%, 8.3%, and 9.5% for the $D_s^+D_{s1}(2536)^-$, $D_s^+D_{s2}(2573)^-$, $D_s^{*+}D_{s1}(2536)^-$, and $D_s^{*+}D_{s2}(2573)^-$, respectively.

	D_s^+ reconstruction						K^-	K_S^0
Source \ D_s^+ decay mode	$\phi\pi^+$	$K_S^0K^+$	$\bar{K}^*(892)^0K^+$	$\rho^+\phi$	$\eta\pi^+(\gamma\gamma/\pi^+\pi^-\pi^0)$	$\eta'\pi^+(\gamma\gamma/\pi^+\pi^-\pi^0)$	K^-	K_S^0
K ID	2.20	1.10	2.20	2.20	—	—	1.10	—
π ID	0.90	—	0.90	0.90	0.90/2.70	2.70/4.50	—	—
Tracking	1.05	1.05	1.05	1.05	0.35/1.05	1.05/1.75	0.35	—
K_S^0 reconstruction	—	2.23	—	—	—	—	—	2.23
π^0 reconstruction	—	—	—	2.25	2.25/—	2.25/—	—	—
Photon reconstruction	—	—	—	—	4.0/—	4.0/—	—	—
Mass windows of intermediate states	0.07	0.20	0.97	1.44	0.23/1.68	0.26/1.69	—	0.20
$\mathcal{B}$s of intermediate state decays	0.08	0.08	0.08	1.12	0.04/0.03	0.04/0.03	—	—
D_s^+ mass window	0.43	0.67	0.19	0.79	1.07	1.20	—	—
D_s^{*+} mass window	0.14	1.01	0.01	0.12	0.89	0.37	—	—

Source \ Reconstruction mode	$D_s^+K^-$	$D_s^+K_S^0$	$D_s^{*+}K^-$	$D_s^{*+}K_S^0$
$D_s^{(*)+}K$ reconstruction	2.2	2.2	2.3	2.3
$\mathcal{B}(D_s^{*+}\to\gamma D_s^+)$	—	—	0.7	0.7
Trigger	1.0	1.0	1.0	1.0
MC statistics	0.2	0.2	0.2	0.2
$N_{\Upsilon(2S)}$ (luminosity)	2.2(1.4)	2.2(1.4)	2.2(1.4)	2.2(1.4)
Sum in quadrature	3.3(2.8)	3.3(2.8)	3.3(2.9)	3.3(2.9)

[1] J. E. Augustin et al., SLAC-SP-017 Collaboration, Phys. Rev. Lett. **37** (1976) 255.

[2] S. Navas et al. (Particle Data Group), Phys. Rev. D **110** (2024) 1030001

[3] S. Godfrey and N. Isgur, Phys. Rev. D **32** (1985) 189.

[4] Stephen Godfrey and Kenneth Moats, Phys. Rev. D **93** (2016) 034035.

[5] P. del Amo Sanchez et al., BaBar Collaboration, Phys. Rev. D **82** (2010) 111101(R).

[6] R. Aaij et al., LHCb Collaboration, Phys. Rev. D **101** (2020) 032005.

[7] B. Aubert et al., BaBaR Collaboration, Phys. Rev. Lett. **90** (2003) 242001.

[8] P. Krokovny et al., Belle Collaboration, Phys. Rev. Lett. **91** (2003) 262002.

[9] J. Brodzicka et al., Belle Collaboration, Phys. Rev. Lett. **100** (2008) 092001.

[10] B. Aubert et al., Belle Collaboration, Phys. Rev. D **80** (2009) 092003.

[11] B.S. Gao et al., Belle Collaboration, Phys. Rev. D **108** (2023) 112015.

[12] X. L. Wang *et al.*, BELLE note #1185.

[13] B. Casey, BELLE note # 390.

[14] K. Inami, BELLE note # 629.

[15] L. Hinz, BELLE note #954, and information from http://belle.kek.jp/group/pid joint/ and discussion with Nishida-san.

[16] Y. Tosa, Report No. DPNU-34-1976, 1976, http://inspirehep .net/record/109354.

[17] R. Brun et al., GEANT 3.21, CERN Report DD/EE/84-1 (1984).

[18] H. Nakano, Ph.D. thesis, Tohoku University, 2014.

[19] M. Feindt and U. Kerzel, NucI. Instrum. Methods Phys. Res., Sect. A 559, 190 (2006).

[20] S. Actis *et al.*, Eur. Phys. J. C **66** (2010) 585.

[21] X. K. Dong, X. H. Mo, P. Wang, and C. Z. Yuan, Chin. Phys. C **44** (2020) 083001.

[22] E. A. Kuraev and V. S. Fadin, Yad. Fiz. **41**, 733(1985) [Sov. J. Nucl. Phys. **41**, 466(1985)].

[23] S. Jadach, B. F. L. Ward, and Z. Was, Phys. Rev. D **63** (2001) 113009; Comput. Phys. Commun. **130**, 260(2000).

[24] M. Benayoun, S. I. Eidelman, V. N. Ivanchenko, and Z. K. Silagadze, Mod. Phys. Lett. A **14**, 2605(1999).

[25] B. Bhuyan et al. BELLE note #1165.

[26] S. Nishida et al. BELLE note #779.

[27] N. Dash et al. BELLE note #1373.

[28] S. Ryu et al. BELLE note #1224.

[29] H. W. Kim et al. BELLE note #499.

[30] Y. P. Guo and C. Z. Yuan, Phys. Rev. D **105** (2022) 114001.

IX. APPENDIX A:VALIDATION CHECKS

In Figs. 9 and 10, we present the distributions of $\bar{K}\bar{D}^{(*)}$ for two data samples. And the Table IV presents the $\sum \varepsilon_i \mathcal{B}_i$ values derived from the signal MC simulations. Due to the strong correlation between the K_S^0 model and the K^- model, this work focuses solely on comparing the results of the K^- model, which are presented in Table VI.

TABLE IV. $\sum \varepsilon_i \mathcal{B}_i$ is the sum of the products of the reconstruction efficiencies and branching fractions in D_s^+'s six decay channels for studying of $\Upsilon(2S)/e^+e^- \to D_s^{(*)+} D_{sJ}^- + c.c.$. In the K_S^0 mode, $\sum \varepsilon_i \mathcal{B}_i$ is multiplied by the branching ratio of $K_S^0 \to \pi^-\pi^+$.

Final states	$\sum \varepsilon_i \mathcal{B}_i$			
	continuum MC simulations		$\Upsilon(2S)$ MC simulations	
	K^- mode (%)	K_S^0 mode (%)	K^- mode (%)	K_S^0 mode (%)
$D_s^+ D_{s1}(2536)^-(\to \bar{D}^* \bar{K})$	1.80 ± 0.03	1.07 ± 0.02	1.69 ± 0.02	0.97 ± 0.01
$D_s^{*+} D_{s1}(2536)^-(\to \bar{D}^* \bar{K})$	1.56 ± 0.02	0.90 ± 0.01	1.53 ± 0.02	0.86 ± 0.01
$D_s^+ D_{s2}(2573)^-(\to \bar{D} \bar{K})$	1.92 ± 0.03	1.22 ± 0.02	1.87 ± 0.03	1.19 ± 0.02
$D_s^{*+} D_{s2}(2573)^-(\to \bar{D} \bar{K})$	1.23 ± 0.02	0.75 ± 0.01	1.17 ± 0.02	0.74 ± 0.01

We determine the numbers of D_{sJ}^- signals, $N^{\rm sig}_{\Upsilon(2S)}$ of the $\Upsilon(2S)$ decays and $N^{\rm sig}_{\rm cont}$ of the continuum production at $\sqrt{s} = 10.52$ GeV, by simultaneously fitting the $M_{\bar{K}\bar{D}^{(*)}}$ distributions for the $\Upsilon(2S)$ data sample and the continuum data sample, and with common isospin ratios $R_{{\rm iso},J} \equiv \mathcal{B}(D_{sJ}^- \to K_S^0 D^{(*)-})/\mathcal{B}(D_{sJ}^- \to K^- \bar{D}^{(*)0})$ between the $K_S^0 D^{(*)-}$ and $K^- \bar{D}^{(*)0}$ final states. In the fits, we use $N^{\rm sig}_{\Upsilon(2S)}$ and $N^{\rm sig}_{\rm cont}$ of the $K^- \bar{D}^{(*)0}$ modes, and those of the $K_S^0 D^{(*)-}$ modes are calculated via the isospin ratios $R_{{\rm iso},J}$ and the ratios of efficiencies and branching fractions between the $K_S^0 D^{(*)-}$ modes and the $K^- \bar{D}^{(*)0}$ modes. The fit function is the sum of a Breit-Wigner function (BW) convolved with a Gaussian function with a width corresponding to the mass resolution, and a linear function to describe the backgrounds. The mass and width of the BW functions are fixed to the world average values for $D_{s1}(2536)^-$ and $D_{s2}(2573)^-$ [2]. Figs. 8 show the mass resolutions used in the Gaussian are obtained from MC simulations and are about 2.8 MeV/c^2 (6.5 MeV/c^2) for $D_{s1}(2536)^-$ ($D_{s2}(2573)^-$). We include the branching fractions and reconstruction efficiencies corresponding to the $D_s^{(*)+} D_{sJ}^-$ final states in the fits.

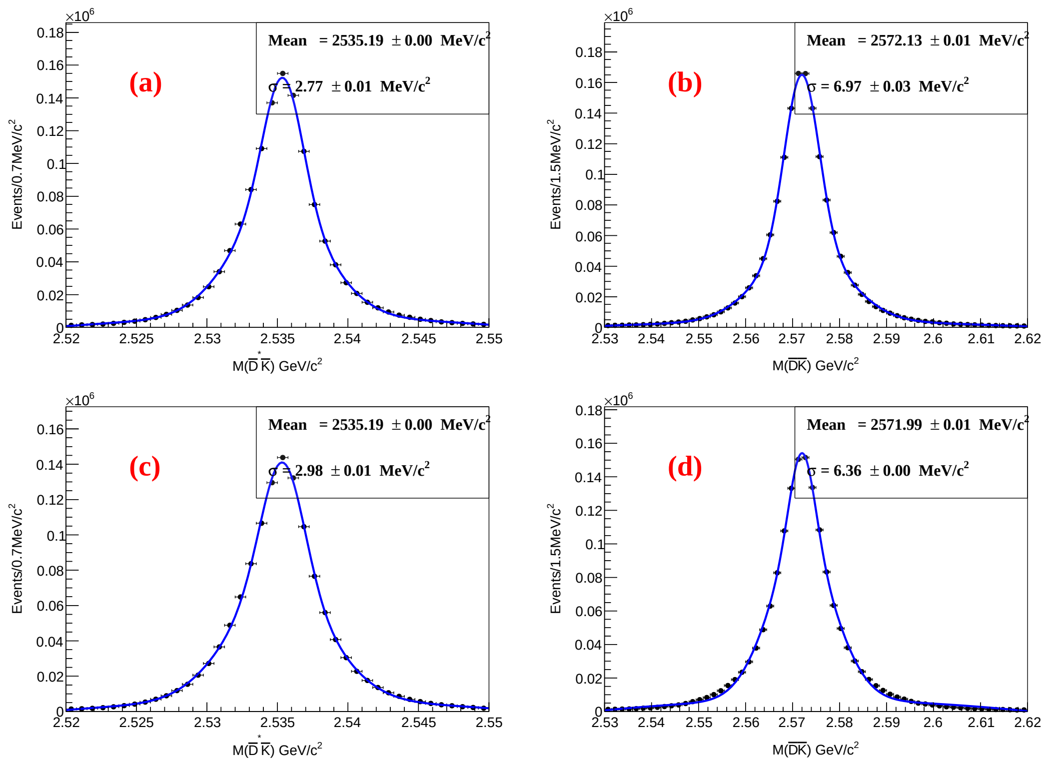

FIG. 8. The invariant mass distributions of $\bar{K}\bar{D}^*$ calculated in the recoil mass for $D_s^{(*)+}$ in the (a)$D_{s1}(2536)^- \to \bar{D}^*\bar{K}$, (b)$D_{s2}(2573)^- \to \bar{D}\bar{K}$ from $\Upsilon(2S)$ signal MC simulations (top panels) and (c-d)the continuum signal MC simulations at 10.52 GeV (bottom panels). The curves show the best fit results using Gaussian functions for the D_s^+ signals.

In principle, there is interference between the resonance and continuum amplitudes in the $\Upsilon(2S)$ data sample [30]. While we do not account for this effect in the simultaneous fit, we do include it as part of the systematic uncertainties, as shown in Table V.

We estimate the contribution of continuum production to the $D_s^{(*)+}D_{sJ}^-$ signal in the $\Upsilon(2S)$ data sample. For this, we scale the luminosities and correct for the center-of-mass (c.m.) energy dependence of the QED cross section, , $\sigma_{e^+e^-} \propto 1/s$. This results in a scale factor of $f_{\rm scale} = (\mathcal{L}_{\Upsilon(2S)} \times s_{\rm cont})/(\mathcal{L}_{\rm cont} \times s_{\Upsilon(2S)}) = 0.304$. Here, $\mathcal{L}_{\Upsilon(2S)}$ and $\mathcal{L}_{\rm cont}$ are the integrated luminosities of the $\Upsilon(2S)$ data sample at $\sqrt{s_{\Upsilon(2S)}} = 10.02$ GeV and the continuum data sample at $\sqrt{s_{\rm cont}} = 10.52$ GeV. Therefore, the yield of signal events produced via continuum e^+e^- annihilation in the $\Upsilon(2S)$ data sample is given by $f_{\rm scale} \times N^{\rm sig}_{\rm cont}$. We determine the statistical significance of D_{sJ}^- by comparing the value of $\Delta(-2\ln L) = -2\ln(L_{\max}/L_0)$ and the change in the number of free parameters in the fits, where $L_{\max}$ is

TABLE V. The parameters $A = \sqrt{\sigma^{\mathrm{B}}(e^+e^- \to D_s^{(*)+} D_{sJ}^-)/\mathcal{B}(\Upsilon(2S) \to D_s^{(*)+} D_{sJ}^-)}$ from the results of the simultaneous fits and the maximum effect of interference $F_{\mathrm{int}}^{\mathrm{max}}$ in the $\Upsilon(2S)$ decays. The $A(K^-)$ and $F_{\mathrm{int}}^{\mathrm{max}}(K^-)$ are the K^- mode.

	$A(K^-)(\mathrm{nb}^{1/2})$		$F_{\mathrm{int}}^{\mathrm{max}}(K^-)(\%)$	
	This work	Published	This work	Published
$D_s^+ D_{s1}(2536)^-$	2.10 ± 0.23	2.05 ± 0.23	8.2	8.0
$D_s^{*+} D_{s1}(2536)^-$	2.04 ± 0.23	2.45 ± 0.38	8.0	9.7
$D_s^+ D_{s2}(2573)^-$	1.80 ± 0.30	2.00 ± 0.32	6.9	8.0
$D_s^{*+} D_{s2}(2573)^-$	2.50 ± 0.50	3.43 ± 0.99	9.8	14.4

the likelihood with D_{sJ}^- and L_0 without D_{sJ}^-.

TABLE VI. The branching fractions of $\Upsilon(2S) \to D_s^{(*)+} D_{sJ}^-$ decays the Born cross sections of continuum production $e^+e^- \to D_s^{(*)+} D_{sJ}^-$, and the isospin ratio $\mathcal{B}(D_{sJ}^- \to K_S^0 D^{(*)-})/\mathcal{B}(D_{sJ}^- \to K^- \bar{D}^{(*)0})$ based on the results from the simultaneous fits. Here, $N^{\rm sig}_{\Upsilon(2S)}$, $N^{\rm sig}_{\rm cont}$, $\mathcal{B}(\Upsilon(2S) \to D_s^{(*)+} D_{sJ}^-)\mathcal{B}(D_{sJ}^- \to \bar{K}\bar{D}^{(*)})$, and $\sigma^{\rm B}(e^+e^- \to D_s^{(*)+} D_{sJ}^-)\mathcal{B}(D_{sJ}^- \to \bar{K}\bar{D}^{(*)})$ are described in Eqs. (4) and (5). $\sum \varepsilon_i \mathcal{B}_i$ is the sum of the products of the reconstruction efficiencies and branching fractions in D_s^+'s six decay channels. The significance is the statistical significance of the $D_s^{(*)+} D_{sJ}^-$ signals with $D_{sJ}^- \to K^- D^{(*)0}$ in $\Upsilon(2S)$ decays and continuum productions. The $K^- D^{(*)0}$ and $K_S^0 D^{(*)-}$ modes of the D_{sJ}^- decays are connected by the isospin ratio $\mathcal{B}(D_{sJ}^- \to K_S^0 D^{(*)-})/\mathcal{B}(D_{sJ}^- \to K^- \bar{D}^{(*)0})$ in the simultaneous fits. The systematic uncertainties of $N^{\rm sig}$ are of the simultaneous fits only.

Final state (f)	$N^{\rm sig}_{\Upsilon(2S)}$		Significance	$\mathcal{B}(\Upsilon(2S) \to D_s^{(*)+} D_{sJ}^-)\mathcal{B}(D_{sJ}^- \to \bar{K}\bar{D}^{(*)})(\times 10^{-5})$	
	This work	Published	(σ)	This work	Published
$D_s^+ D_{s1}(2536)^-$	$39 \pm 10 \pm 1$	$43 \pm 9 \pm 2$	4.6	$1.5 \pm 0.3 \pm 0.2$	$1.6 \pm 0.3 \pm 0.2$
$D_s^{*+} D_{s1}(2536)^-$	$43 \pm 10 \pm 1$	$31 \pm 8 \pm 2$	5.2	$1.8 \pm 0.4 \pm 0.2$	$1.4 \pm 0.4 \pm 0.2$
$D_s^+ D_{s2}(2573)^-$	$52 \pm 14 \pm 3$	$51 \pm 15 \pm 5$	4.0	$1.8 \pm 0.5 \pm 0.2$	$1.4 \pm 0.4 \pm 0.2$
$D_s^{*+} D_{s2}(2573)^-$	$36 \pm 14 \pm 1$	$20 \pm 14 \pm 2$	2.9	$1.9 \pm 0.8 \pm 0.3$	$0.9 \pm 0.5 \pm 0.2$
—	$N^{\rm sig}_{\rm cont}$		—	$\sigma^{\rm B}(e^+e^- \to D_s^{(*)+} D_{sJ}^-)\mathcal{B}(D_{sJ}^- \to \bar{K}\bar{D})$(fb)	
	This work	Published		This work	Published
$D_s^+ D_{s1}(2536)^-$	$95 \pm 11 \pm 2$	$86 \pm 10 \pm 2$	13.2	$67 \pm 8 \pm 1$	$67 \pm 8 \pm 6$
$D_s^{*+} D_{s1}(2536)^-$	$95 \pm 11 \pm 2$	$79 \pm 10 \pm 2$	12.7	$77 \pm 9 \pm 1$	$84 \pm 11 \pm 11$
$D_s^+ D_{s2}(2573)^-$	$75 \pm 16 \pm 6$	$102 \pm 17 \pm 21$	5.2	$55 \pm 11 \pm 4$	$56 \pm 9 \pm 13$
$D_s^{*+} D_{s2}(2573)^-$	$134 \pm 19 \pm 3$	$102 \pm 16 \pm 6$	8.3	$139 \pm 20 \pm 3$	$106 \pm 17 \pm 12$

Isospin ratio $\mathcal{B}(D_{sJ}^- \to K_S^0 D^{(*)-})/\mathcal{B}(D_{sJ}^- \to K^- \bar{D}^{(*)0})$		
D_{sJ}^-	This work	Published
$D_{s1}(2536)^-$ decays	$0.40 \pm 0.06 \pm 0.02$	$0.48 \pm 0.07 \pm 0.02$
$D_{s2}(2573)^-$ decays	$0.50 \pm 0.10 \pm 0.02$	$0.48 \pm 0.07 \pm 0.02$

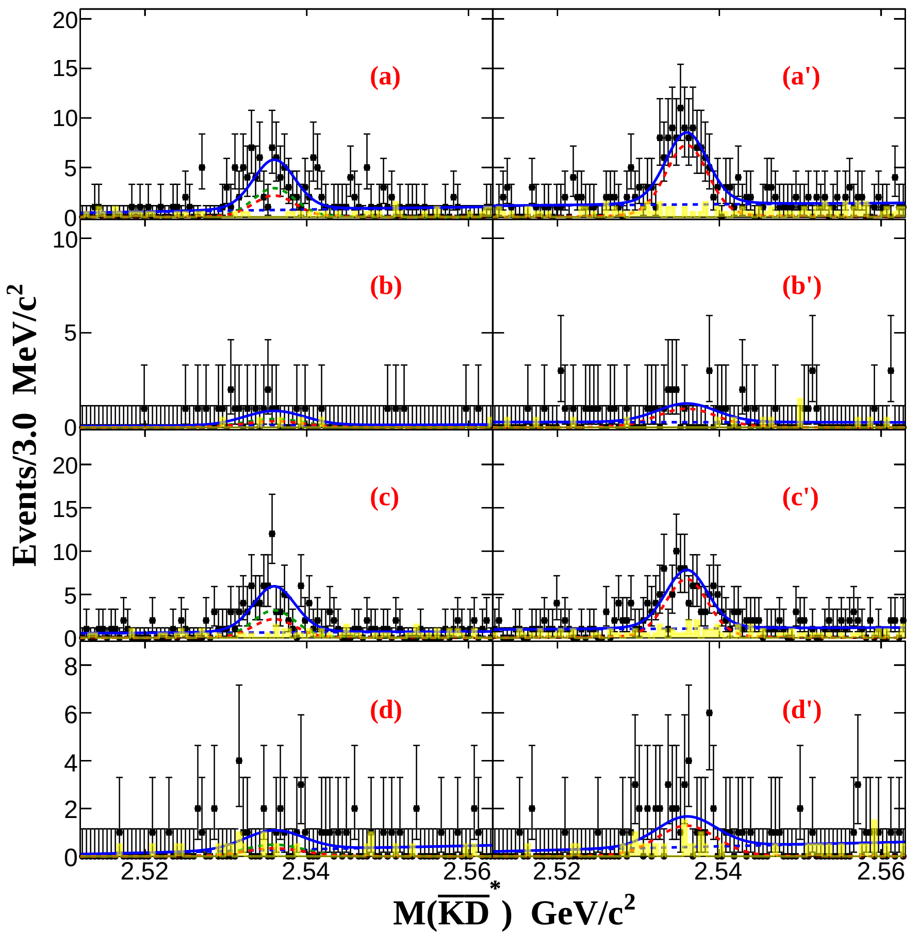

FIG. 9. The invariant mass distributions of $\bar{K}\bar{D}^*$ calculated in the recoil mass for $D_s^{(*)+}$ in the (a) $D_s^+K^-\bar{D}^*(2007)^0$, (b) $D_s^+K_S^0D^*(2010)^+$, (c) $D_s^{*+}K^-\bar{D}^*(2007)^0$, and (d) $D_s^{*+}K_S^0D^*(2010)^+$ final states from the $\Upsilon(2S)$ data sample (left panels) and the continuum data sample at 10.52 GeV (right panels). The shaded histograms show the backgrounds estimated from the normalized $D_s^{(*)+}$ mass sidebands. The solid curves show the best fit result; the dashed green ones are $D_{s1}(2536)^-$ signals in $\Upsilon(2S)$ decays, and the dashed red curves are the $D_{s1}(2536)^-$ signals in continuum production at 10.02 GeV (left panels) and 10.52 GeV (right panels).

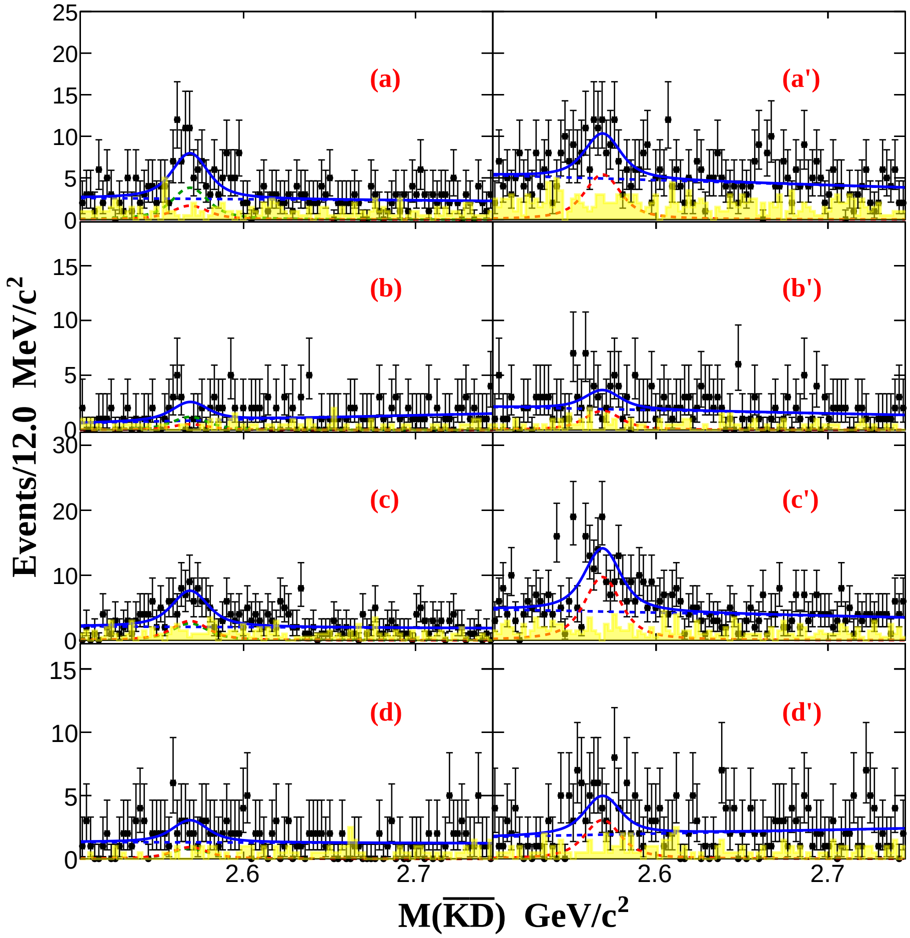

FIG. 10. The invariant mass distributions of $\bar{K}\bar{D}$ calculated in recoil mass for $D_s^{(*)+}$ in the (a) $D_s^+K^-\bar{D}^0$, (b) $D_s^+K_S^0D^-$, (c) $D_s^{*+}K^-\bar{D}^0$, and (d) $D_s^{*+}K_S^0D^-$ final states from the $\Upsilon(2S)$ data sample (left panels) and the continuum data sample at 10.52 GeV (right panels). The shaded histograms show the backgrounds estimated from the normalized $D_s^{(*)+}$ mass sidebands. The solid curves show the best fit result; the dashed green ones are $D_{s2}(2573)^-$ signals in $\Upsilon(2S)$ decays, and the dashed red curves are the $D_{s2}(2573)^-$ signals in continuum production at 10.02 GeV (left panels) and 10.52 GeV (right panels).

X. APPENDIX B: THE FITTING PARAMETERS OF RECOIL MASS SPECTRA AGAINST $D_s^{(*)+}$ IN EACH D_s^+ DECAY MODE

Table VII- XIV present the fitting parameters of the recoil mass spectra against $D_s^{(*)+}$ in each D_s^+ decay mode, utilized in the study of the $\Upsilon(2S)/e^+e^- \to D_s^{(*)+}D_{sJ}^-(\to \bar{D}^{(*)}\bar{K})$, where D_{sJ}^- can be either $D_{s1}^*(2700)^-$ or $D_{s1}^*(2860)^-$.

TABLE VII. Reconstruction efficiencies (ε), branching fractions($\mathcal{B}$), and their product $\varepsilon\times\mathcal{B}$) for each reconstructed D_s^+ are presented for the study of $\Upsilon(2S)/e^+e^- \to D_s^+D_{s1}^*(2700)^-(\to \bar{D}^*\bar{K})$. Here, $\bar{D}^*\bar{K}$ is $\bar{D}^{*0}K^-$ or $D^{*-}K_S^0$.

$\Upsilon(2S) \to D_s^+D_{s1}^*(2700)^-(\to \bar{D}^*\bar{K})$					
D_s^+ mode	$\mathcal{B}(\%)$	K^-		K_S^0	
		$\varepsilon(\%)$	$\varepsilon\times\mathcal{B}(\%)$	$\varepsilon(\%)$	$\varepsilon\times\mathcal{B}(\%)$
$\phi\pi^+$	2.21 ± 0.06	20.54 ± 0.06	0.45 ± 0.01	18.37 ± 0.06	0.41 ± 0.01
$K_S^0K^+$	1.01 ± 0.02	23.70 ± 0.10	0.24 ± 0.00	20.85 ± 0.10	0.21 ± 0.00
$\bar{K}^*(892)^0K^+$	2.58 ± 0.06	20.50 ± 0.06	0.53 ± 0.01	18.18 ± 0.06	0.47 ± 0.01
$\rho^+\phi$	2.74 ± 0.17	8.18 ± 0.04	0.22 ± 0.01	7.26 ± 0.04	0.20 ± 0.01
$\eta\pi^+$	1.05 ± 0.05	14.62 ± 0.08	0.15 ± 0.01	12.78 ± 0.07	0.13 ± 0.01
$\eta'\pi^+$	1.05 ± 0.05	11.08 ± 0.07	0.12 ± 0.01	10.13 ± 0.07	0.11 ± 0.01

$e^+e^- \to D_s^+D_{s1}^*(2700)^-(\to \bar{D}^*\bar{K})$					
D_s^+ mode	$\mathcal{B}(\%)$	K^-		K_S^0	
		$\varepsilon(\%)$	$\varepsilon\times\mathcal{B}(\%)$	$\varepsilon(\%)$	$\varepsilon\times\mathcal{B}(\%)$
$\phi\pi^+$	2.21 ± 0.06	20.96 ± 0.06	0.46 ± 0.01	18.78 ± 0.06	0.42 ± 0.01
$K_S^0K^+$	1.01 ± 0.02	23.73 ± 0.10	0.24 ± 0.00	20.82 ± 0.10	0.21 ± 0.00
$\bar{K}^*(892)^0K^+$	2.58 ± 0.06	20.98 ± 0.06	0.54 ± 0.01	18.86 ± 0.06	0.49 ± 0.01
$\rho^+\phi$	2.74 ± 0.17	8.26 ± 0.04	0.23 ± 0.01	7.46 ± 0.04	0.20 ± 0.01
$\eta\pi^+$	1.05 ± 0.05	15.30 ± 0.08	0.16 ± 0.01	12.25 ± 0.07	0.13 ± 0.01
$\eta'\pi^+$	1.05 ± 0.05	11.90 ± 0.07	0.12 ± 0.01	9.90 ± 0.07	0.10 ± 0.00

TABLE VIII. Reconstruction efficiencies (ε), branching fractions($\mathcal{B}$), and their product $\varepsilon \times \mathcal{B}$) for each reconstructed D_s^+ are presented for the study of $\Upsilon(2S)/e^+e^- \to D_s^{*+} D_{s1}^*(2700)^-(\to \bar{D}^* \bar{K})$. Here, $\bar{D}^* \bar{K}$ is $\bar{D}^{*0} K^-$ or $D^{*-} K_S^0$.

$\Upsilon(2S) \to D_s^{*+} D_{s1}^*(2700)^-(\to \bar{D}^* \bar{K})$					
D_s^+ mode	$\mathcal{B}(\%)$	K^-		K_S^0	
		$\varepsilon(\%)$	$\varepsilon \times \mathcal{B}(\%)$	$\varepsilon(\%)$	$\varepsilon \times \mathcal{B}(\%)$
$\phi\pi^+$	2.07 ± 0.06	22.87 ± 0.06	0.47 ± 0.01	17.87 ± 0.06	0.37 ± 0.01
$K_S^0 K^+$	0.94 ± 0.02	23.87 ± 0.10	0.23 ± 0.00	20.62 ± 0.10	0.19 ± 0.00
$\bar{K}^*(892)^0 K^+$	2.41 ± 0.06	21.40 ± 0.06	0.52 ± 0.01	18.25 ± 0.06	0.44 ± 0.01
$\rho^+\phi$	2.56 ± 0.16	5.75 ± 0.03	0.15 ± 0.01	4.76 ± 0.03	0.12 ± 0.01
$\eta\pi^+$	0.98 ± 0.05	12.07 ± 0.07	0.12 ± 0.01	10.62 ± 0.07	0.10 ± 0.01
$\eta'\pi^+$	0.98 ± 0.05	7.53 ± 0.06	0.07 ± 0.00	6.41 ± 0.05	0.06 ± 0.00
$e^+e^- \to D_s^{*+} D_{s1}^*(2700)^-(\to \bar{D}^* \bar{K})$					
D_s^+ mode	$\mathcal{B}(\%)$	K^-		K_S^0	
		$\varepsilon(\%)$	$\varepsilon \times \mathcal{B}(\%)$	$\varepsilon(\%)$	$\varepsilon \times \mathcal{B}(\%)$
$\phi\pi^+$	2.07 ± 0.06	22.66 ± 0.06	0.47 ± 0.01	18.08 ± 0.06	0.37 ± 0.01
$K_S^0 K^+$	0.94 ± 0.02	23.80 ± 0.10	0.22 ± 0.00	20.01 ± 0.09	0.19 ± 0.00
$\bar{K}^*(892)^0 K^+$	2.41 ± 0.06	21.26 ± 0.06	0.51 ± 0.01	18.33 ± 0.06	0.44 ± 0.01
$\rho^+\phi$	2.56 ± 0.16	5.59 ± 0.03	0.14 ± 0.01	4.80 ± 0.03	0.12 ± 0.01
$\eta\pi^+$	0.98 ± 0.05	11.84 ± 0.07	0.12 ± 0.01	10.32 ± 0.07	0.10 ± 0.01
$\eta'\pi^+$	0.98 ± 0.05	7.29 ± 0.06	0.07 ± 0.00	6.26 ± 0.05	0.06 ± 0.00

TABLE IX. Reconstruction efficiencies (ε), branching fractions($\mathcal{B}$), and their product $\varepsilon \times \mathcal{B}$) for each reconstructed D_s^+ are presented for the study of $\Upsilon(2S)/e^+e^- \to D_s^+ D_{s1}^*(2700)^-(\to \bar{D}\bar{K})$. Here, $\bar{D}\bar{K}$ is $\bar{D}^0 K^-$ or $D^- K_S^0$.

$\Upsilon(2S) \to D_s^{*+} D_{s1}^*(2700)^-(\to \bar{D}\bar{K})$					
D_s^+ mode	$\mathcal{B}(\%)$	K^-		K_S^0	
		$\varepsilon(\%)$	$\varepsilon \times \mathcal{B}(\%)$	$\varepsilon(\%)$	$\varepsilon \times \mathcal{B}(\%)$
$\phi\pi^+$	2.21 ± 0.06	17.24 ± 0.06	0.38 ± 0.01	16.02 ± 0.06	0.35 ± 0.01
$K_S^0 K^+$	1.01 ± 0.02	19.53 ± 0.09	0.20 ± 0.00	17.47 ± 0.09	0.18 ± 0.00
$\bar{K}^*(892)^0 K^+$	2.58 ± 0.06	17.17 ± 0.05	0.44 ± 0.01	15.68 ± 0.05	0.40 ± 0.01
$\rho^+\phi$	2.74 ± 0.17	6.18 ± 0.03	0.17 ± 0.01	5.64 ± 0.03	0.15 ± 0.01
$\eta\pi^+$	1.05 ± 0.05	9.40 ± 0.07	0.10 ± 0.00	8.95 ± 0.06	0.09 ± 0.00
$\eta'\pi^+$	1.05 ± 0.05	8.03 ± 0.06	0.08 ± 0.00	7.51 ± 0.06	0.08 ± 0.00

$e^+e^- \to D_s^{*+} D_{s1}^*(2700)^-(\to \bar{D}\bar{K})$					
D_s^+ mode	$\mathcal{B}(\%)$	K^-		K_S^0	
		$\varepsilon(\%)$	$\varepsilon \times \mathcal{B}(\%)$	$\varepsilon(\%)$	$\varepsilon \times \mathcal{B}(\%)$
$\phi\pi^+$	2.21 ± 0.06	17.87 ± 0.06	0.39 ± 0.01	16.17 ± 0.06	0.36 ± 0.01
$K_S^0 K^+$	1.01 ± 0.02	19.71 ± 0.09	0.20 ± 0.00	18.08 ± 0.09	0.18 ± 0.00
$\bar{K}^*(892)^0 K^+$	2.58 ± 0.06	17.86 ± 0.06	0.46 ± 0.01	15.99 ± 0.05	0.41 ± 0.01
$\rho^+\phi$	2.74 ± 0.17	5.97 ± 0.03	0.16 ± 0.01	5.56 ± 0.03	0.15 ± 0.01
$\eta\pi^+$	1.05 ± 0.05	10.41 ± 0.07	0.11 ± 0.01	8.20 ± 0.06	0.09 ± 0.00
$\eta'\pi^+$	1.05 ± 0.05	9.00 ± 0.06	0.09 ± 0.00	7.82 ± 0.06	0.08 ± 0.00

TABLE X. Reconstruction efficiencies (ε), branching fractions($\mathcal{B}$), and their product $\varepsilon \times \mathcal{B}$) for each reconstructed D_s^+ are presented for the study of $\Upsilon(2S)/e^+e^- \to D_s^{*+} D_{s1}^*(2700)^-(\to \bar{D}\bar{K})$. Here, $\bar{D}\bar{K}$ is $\bar{D}^0 K^-$ or $D^- K_S^0$.

$\Upsilon(2S) \to D_s^{*+} D_{s1}^*(2700)^-(\to \bar{D}\bar{K})$					
D_s^+ mode	$\mathcal{B}(\%)$	K^-		K_S^0	
		$\varepsilon(\%)$	$\varepsilon \times \mathcal{B}(\%)$	$\varepsilon(\%)$	$\varepsilon \times \mathcal{B}(\%)$
$\phi\pi^+$	2.07 ± 0.06	17.46 ± 0.06	0.36 ± 0.01	15.45 ± 0.06	0.36 ± 0.01
$K_S^0 K^+$	0.94 ± 0.02	18.80 ± 0.09	0.18 ± 0.00	17.01 ± 0.09	0.18 ± 0.00
$\bar{K}^*(892)^0 K^+$	2.41 ± 0.06	17.06 ± 0.05	0.41 ± 0.01	15.38 ± 0.05	0.41 ± 0.01
$\rho^+\phi$	2.56 ± 0.16	4.20 ± 0.03	0.11 ± 0.01	3.80 ± 0.03	0.11 ± 0.01
$\eta\pi^+$	0.98 ± 0.05	8.71 ± 0.06	0.09 ± 0.00	7.08 ± 0.06	0.09 ± 0.00
$\eta'\pi^+$	0.98 ± 0.05	4.84 ± 0.05	0.05 ± 0.00	4.48 ± 0.05	0.05 ± 0.00

$e^+e^- \to D_s^{*+} D_{s1}^*(2700)^-(\to \bar{D}\bar{K})$					
D_s^+ mode	$\mathcal{B}(\%)$	K^-		K_S^0	
		$\varepsilon(\%)$	$\varepsilon \times \mathcal{B}(\%)$	$\varepsilon(\%)$	$\varepsilon \times \mathcal{B}(\%)$
$\phi\pi^+$	2.07 ± 0.06	17.83 ± 0.06	0.37 ± 0.01	15.63 ± 0.06	0.32 ± 0.01
$K_S^0 K^+$	0.94 ± 0.02	18.49 ± 0.09	0.17 ± 0.00	17.24 ± 0.09	0.16 ± 0.00
$\bar{K}^*(892)^0 K^+$	2.41 ± 0.06	17.21 ± 0.05	0.42 ± 0.01	15.50 ± 0.05	0.37 ± 0.01
$\rho^+\phi$	2.56 ± 0.16	4.05 ± 0.03	0.10 ± 0.01	3.92 ± 0.03	0.10 ± 0.01
$\eta\pi^+$	0.98 ± 0.05	7.24 ± 0.06	0.07 ± 0.00	6.67 ± 0.06	0.07 ± 0.00
$\eta'\pi^+$	0.98 ± 0.05	5.59 ± 0.05	0.05 ± 0.00	4.41 ± 0.05	0.04 ± 0.00

TABLE XI. Reconstruction efficiencies (ε), branching fractions($\mathcal{B}$), and their product $\varepsilon \times \mathcal{B}$) for each reconstructed D_s^+ are presented for the study of $\Upsilon(2S)/e^+e^- \to D_s^+ D_{s1}^*(2860)^-(\to \bar{D}^* \bar{K})$. Here, $\bar{D}^* \bar{K}$ is $\bar{D}^{*0} K^-$ or $D^{*-} K_S^0$.

$\Upsilon(2S) \to D_s^+ D_{s1}^*(2860)^-(\to \bar{D}^* \bar{K})$					
D_s^+ mode	$\mathcal{B}(\%)$	K^-		K_S^0	
		$\varepsilon(\%)$	$\varepsilon \times \mathcal{B}(\%)$	$\varepsilon(\%)$	$\varepsilon \times \mathcal{B}(\%)$
$\phi\pi^+$	2.21 ± 0.06	21.74 ± 0.06	0.48 ± 0.01	18.93 ± 0.06	0.42 ± 0.01
$K_S^0 K^+$	1.01 ± 0.02	24.31 ± 0.10	0.25 ± 0.00	21.38 ± 0.10	0.22 ± 0.00
$\bar{K}^*(892)^0 K^+$	2.58 ± 0.06	21.30 ± 0.06	0.55 ± 0.01	18.67 ± 0.06	0.48 ± 0.01
$\rho^+\phi$	2.74 ± 0.17	9.20 ± 0.04	0.25 ± 0.02	8.00 ± 0.04	0.22 ± 0.01
$\eta\pi^+$	1.05 ± 0.05	16.51 ± 0.08	0.17 ± 0.01	14.66 ± 0.08	0.15 ± 0.01
$\eta'\pi^+$	1.05 ± 0.05	13.17 ± 0.08	0.14 ± 0.01	11.27 ± 0.07	0.12 ± 0.01

$e^+e^- \to D_s^+ D_{s1}^*(2860)^-(\to \bar{D}^* \bar{K})$					
D_s^+ mode	$\mathcal{B}(\%)$	K^-		K_S^0	
		$\varepsilon(\%)$	$\varepsilon \times \mathcal{B}(\%)$	$\varepsilon(\%)$	$\varepsilon \times \mathcal{B}(\%)$
$\phi\pi^+$	2.21 ± 0.06	22.14 ± 0.06	0.49 ± 0.01	19.61 ± 0.06	0.43 ± 0.01
$K_S^0 K^+$	1.01 ± 0.02	25.50 ± 0.10	0.26 ± 0.00	22.53 ± 0.10	0.23 ± 0.00
$\bar{K}^*(892)^0 K^+$	2.58 ± 0.06	22.24 ± 0.06	0.57 ± 0.01	19.57 ± 0.06	0.50 ± 0.01
$\rho^+\phi$	2.74 ± 0.17	9.62 ± 0.04	0.26 ± 0.02	8.56 ± 0.04	0.23 ± 0.01
$\eta\pi^+$	1.05 ± 0.05	16.05 ± 0.08	0.17 ± 0.01	14.26 ± 0.08	0.15 ± 0.01
$\eta'\pi^+$	1.05 ± 0.05	13.63 ± 0.08	0.14 ± 0.01	11.80 ± 0.07	0.12 ± 0.01

TABLE XII. Reconstruction efficiencies (ε), branching fractions($\mathcal{B}$), and their product $\varepsilon \times \mathcal{B}$) for each reconstructed D_s^+ are presented for the study of $\Upsilon(2S)/e^+e^- \to D_s^{*+}D_{s1}^*(2860)^-(\to \bar{D}^*\bar{K})$. Here, $\bar{D}^*\bar{K}$ is $\bar{D}^{*0}K^-$ or $D^{*-}K_S^0$.

$\Upsilon(2S) \to D_s^{*+}D_{s1}^*(2860)^-(\to \bar{D}^*\bar{K})$					
D_s^+ mode	$\mathcal{B}(\%)$	K^-		K_S^0	
		$\varepsilon(\%)$	$\varepsilon \times \mathcal{B}(\%)$	$\varepsilon(\%)$	$\varepsilon \times \mathcal{B}(\%)$
$\phi\pi^+$	2.07 ± 0.06	22.61 ± 0.06	0.47 ± 0.01	18.29 ± 0.06	0.38 ± 0.01
$K_S^0K^+$	0.94 ± 0.02	24.40 ± 0.10	0.23 ± 0.00	21.18 ± 0.10	0.20 ± 0.00
$\bar{K}^*(892)^0K^+$	2.41 ± 0.06	21.33 ± 0.06	0.51 ± 0.01	18.44 ± 0.06	0.44 ± 0.01
$\rho^+\phi$	2.56 ± 0.16	5.50 ± 0.03	0.14 ± 0.01	4.75 ± 0.03	0.12 ± 0.01
$\eta\pi^+$	0.98 ± 0.05	13.30 ± 0.08	0.13 ± 0.01	11.69 ± 0.07	0.11 ± 0.01
$\eta'\pi^+$	0.98 ± 0.05	7.86 ± 0.06	0.08 ± 0.00	6.70 ± 0.06	0.07 ± 0.00
$e^+e^- \to D_s^{*+}D_{s1}^*(2860)^-(\to \bar{D}^*\bar{K})$					
D_s^+ mode	$\mathcal{B}(\%)$	K^-		K_S^0	
		$\varepsilon(\%)$	$\varepsilon \times \mathcal{B}(\%)$	$\varepsilon(\%)$	$\varepsilon \times \mathcal{B}(\%)$
$\phi\pi^+$	2.07 ± 0.06	23.78 ± 0.07	0.49 ± 0.01	18.89 ± 0.06	0.39 ± 0.01
$K_S^0K^+$	0.94 ± 0.02	24.57 ± 0.10	0.23 ± 0.01	21.94 ± 0.09	0.21 ± 0.00
$\bar{K}^*(892)^0K^+$	2.41 ± 0.06	21.22 ± 0.06	0.51 ± 0.01	19.18 ± 0.06	0.46 ± 0.01
$\rho^+\phi$	2.56 ± 0.16	5.82 ± 0.03	0.15 ± 0.01	4.73 ± 0.03	0.12 ± 0.01
$\eta\pi^+$	0.98 ± 0.05	14.31 ± 0.08	0.14 ± 0.01	11.70 ± 0.07	0.11 ± 0.01
$\eta'\pi^+$	0.98 ± 0.05	7.79 ± 0.06	0.08 ± 0.00	7.02 ± 0.06	0.07 ± 0.00

TABLE XIII. Reconstruction efficiencies (ε), branching fractions($\mathcal{B}$), and their product $\varepsilon \times \mathcal{B}$) for each reconstructed D_s^+ are presented for the study of $\Upsilon(2S)/e^+e^- \to D_s^+ D_{s1}^*(2860)^-(\to \bar{D}\bar{K})$. Here, $\bar{D}\bar{K}$ is $\bar{D}^0 K^-$ or $D^- K_S^0$.

$\Upsilon(2S) \to D_s^{*+} D_{s1}^*(2860)^-(\to \bar{D}\bar{K})$					
D_s^+ mode	$\mathcal{B}(\%)$	K^-		K_S^0	
		$\varepsilon(\%)$	$\varepsilon \times \mathcal{B}(\%)$	$\varepsilon(\%)$	$\varepsilon \times \mathcal{B}(\%)$
$\phi\pi^+$	2.21 ± 0.06	18.25 ± 0.06	0.40 ± 0.01	17.13 ± 0.06	0.40 ± 0.01
$K_S^0 K^+$	1.01 ± 0.02	20.29 ± 0.09	0.20 ± 0.00	18.23 ± 0.09	0.20 ± 0.00
$\bar{K}^*(892)^0 K^+$	2.58 ± 0.06	18.26 ± 0.06	0.47 ± 0.01	16.94 ± 0.06	0.47 ± 0.01
$\rho^+\phi$	2.74 ± 0.17	7.63 ± 0.04	0.21 ± 0.01	6.90 ± 0.04	0.21 ± 0.01
$\eta\pi^+$	1.05 ± 0.05	12.59 ± 0.07	0.13 ± 0.01	10.90 ± 0.07	0.13 ± 0.01
$\eta'\pi^+$	1.05 ± 0.05	10.64 ± 0.07	0.11 ± 0.01	9.56 ± 0.07	0.11 ± 0.01

$e^+e^- \to D_s^{*+} D_{s1}^*(2860)^-(\to \bar{D}\bar{K})$					
D_s^+ mode	$\mathcal{B}(\%)$	K^-		K_S^0	
		$\varepsilon(\%)$	$\varepsilon \times \mathcal{B}(\%)$	$\varepsilon(\%)$	$\varepsilon \times \mathcal{B}(\%)$
$\phi\pi^+$	2.21 ± 0.06	17.87 ± 0.06	0.39 ± 0.01	17.62 ± 0.06	0.39 ± 0.01
$K_S^0 K^+$	1.01 ± 0.02	19.71 ± 0.09	0.20 ± 0.00	19.41 ± 0.09	0.20 ± 0.00
$\bar{K}^*(892)^0 K^+$	2.58 ± 0.06	17.86 ± 0.06	0.46 ± 0.01	17.44 ± 0.05	0.45 ± 0.01
$\rho^+\phi$	2.74 ± 0.17	5.97 ± 0.03	0.16 ± 0.01	7.11 ± 0.04	0.19 ± 0.01
$\eta\pi^+$	1.05 ± 0.05	10.41 ± 0.07	0.11 ± 0.01	10.58 ± 0.07	0.11 ± 0.01
$\eta'\pi^+$	1.05 ± 0.05	9.00 ± 0.06	0.09 ± 0.00	9.90 ± 0.07	0.10 ± 0.00

TABLE XIV. Reconstruction efficiencies (ε), branching fractions($\mathcal{B}$), and their product $\varepsilon \times \mathcal{B}$) for each reconstructed D_s^+ are presented for the study of $\Upsilon(2S)/e^+e^- \to D_s^{*+}D_{s1}^*(2860)^-(\to \bar{D}\bar{K})$. Here, $\bar{D}\bar{K}$ is $\bar{D}^0K^-$ or $D^-K_S^0$.

$\Upsilon(2S) \to D_s^{*+}D_{s1}^*(2860)^-(\to \bar{D}\bar{K})$					
D_s^+ mode	$\mathcal{B}(\%)$	K^-		K_S^0	
		$\varepsilon(\%)$	$\varepsilon \times \mathcal{B}(\%)$	$\varepsilon(\%)$	$\varepsilon \times \mathcal{B}(\%)$
$\phi\pi^+$	2.07 ± 0.06	18.19 ± 0.06	0.38 ± 0.01	15.72 ± 0.06	0.32 ± 0.01
$K_S^0K^+$	0.94 ± 0.02	19.62 ± 0.09	0.19 ± 0.00	17.90 ± 0.09	0.17 ± 0.00
$\bar{K}^*(892)^0K^+$	2.41 ± 0.06	17.88 ± 0.06	0.43 ± 0.01	16.25 ± 0.05	0.39 ± 0.01
$\rho^+\phi$	2.56 ± 0.16	4.67 ± 0.03	0.12 ± 0.01	4.19 ± 0.03	0.11 ± 0.01
$\eta\pi^+$	0.98 ± 0.05	9.33 ± 0.07	0.09 ± 0.00	9.20 ± 0.06	0.09 ± 0.00
$\eta'\pi^+$	0.98 ± 0.05	6.24 ± 0.05	0.06 ± 0.00	5.44 ± 0.05	0.05 ± 0.00

$e^+e^- \to D_s^{*+}D_{s1}^*(2860)^-(\to \bar{D}\bar{K})$					
D_s^+ mode	$\mathcal{B}(\%)$	K^-		K_S^0	
		$\varepsilon(\%)$	$\varepsilon \times \mathcal{B}(\%)$	$\varepsilon(\%)$	$\varepsilon \times \mathcal{B}(\%)$
$\phi\pi^+$	2.07 ± 0.06	18.83 ± 0.06	0.39 ± 0.01	16.54 ± 0.06	0.34 ± 0.01
$K_S^0K^+$	0.94 ± 0.02	20.59 ± 0.09	0.19 ± 0.00	18.72 ± 0.09	0.18 ± 0.00
$\bar{K}^*(892)^0K^+$	2.41 ± 0.06	18.38 ± 0.05	0.44 ± 0.01	16.70 ± 0.05	0.40 ± 0.01
$\rho^+\phi$	2.56 ± 0.16	4.83 ± 0.03	0.12 ± 0.01	4.17 ± 0.03	0.11 ± 0.01
$\eta\pi^+$	0.98 ± 0.05	10.04 ± 0.06	0.10 ± 0.01	9.27 ± 0.06	0.09 ± 0.00
$\eta'\pi^+$	0.98 ± 0.05	6.34 ± 0.05	0.06 ± 0.00	5.88 ± 0.05	0.06 ± 0.00

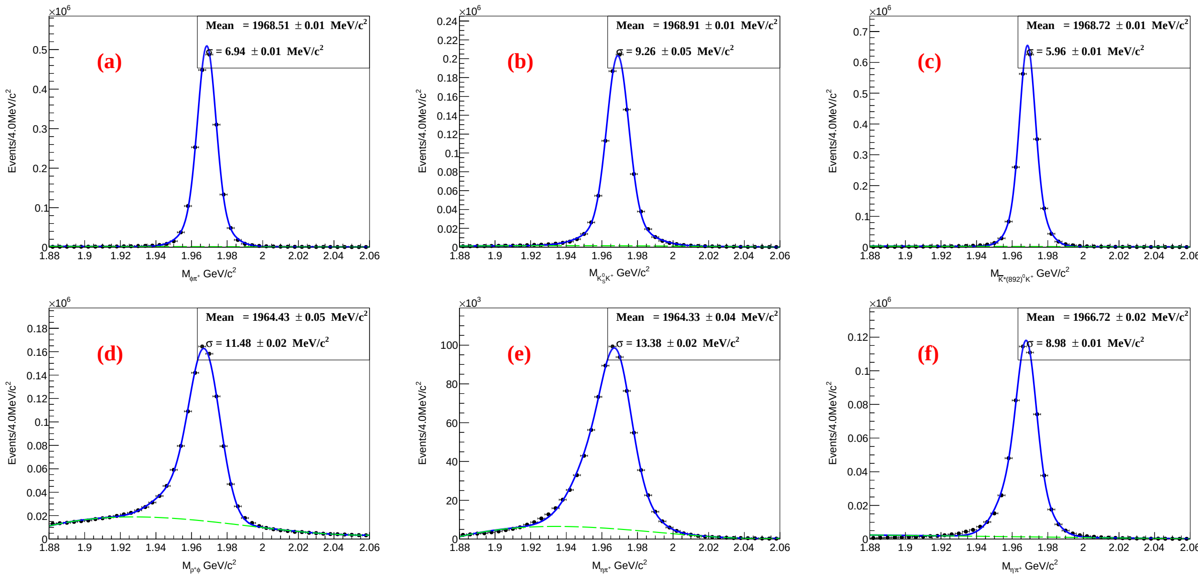

FIG. 11. The invariant mass distributions of the (a)$\phi\pi^+$, (b)$K_S^0K^+$, (c)$K^*(892)^0K^+$, (d)$\phi\rho^+$, (e)$\eta\pi^+$, (f)$\eta'\pi^+$ in the $\Upsilon(2S)$ MC simulations, respectively. The curves show the best fit results using Gaussian functions for the D_s^+ signals.

XI. APPENDIX C: THE DISTRIBUTIONS OF INVARIANT MASS FOR D_s^+ CANDIDATES IN THEIR EACH DECAY MODE

In Appendix C, we present the distributions of invariant mass for D_s^+ and D_s^{*+} candidates ($M_{h_1h_2}/M_{D_s^+\gamma}$). Figs. 11- 14 and Figs. 15- 18 illustrate the distributions of $M_{h_1h_2}$ and $M_{D_s^+\gamma}$ for each D_s^+ decay mode across the $\Upsilon(2S)$ MC simulations, $\Upsilon(2S)$ data samples, continuum MC simulaitions and continuum data samples, respectively.

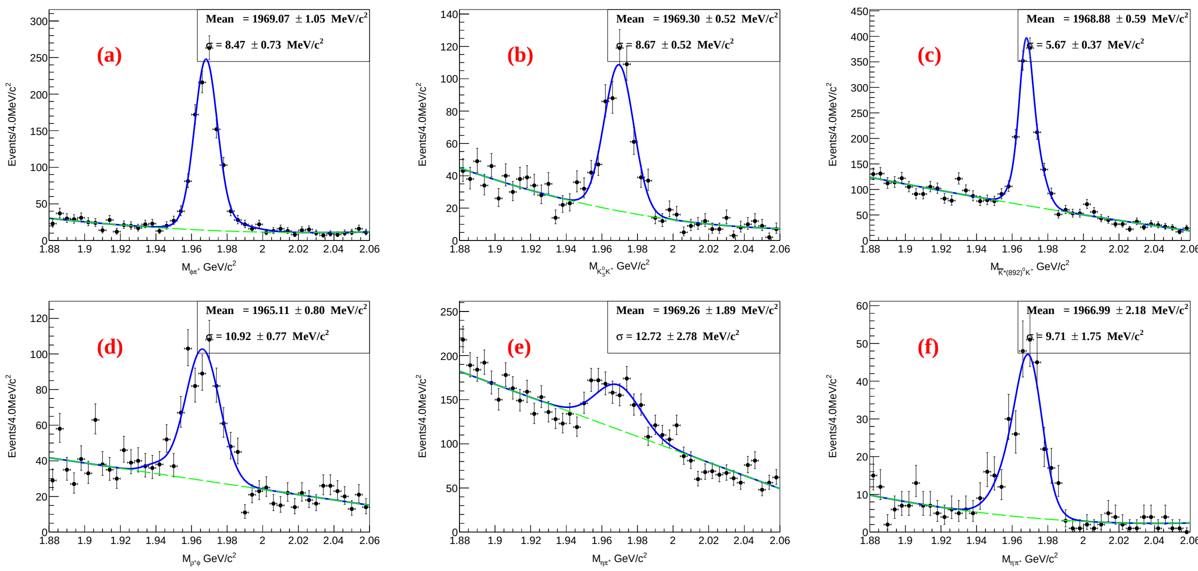

FIG. 12. The invariant mass distributions of the (a)$\phi\pi^+$, (b)$K_S^0K^+$, (c)$K^*(892)^0K^+$, (d)$\phi\rho^+$, (e)$\eta\pi^+$, (f)$\eta'\pi^+$ in the $\Upsilon(2S)$ data samples, respectively. The curves show the best fit results using Gaussian functions for the D_s^+ signals.

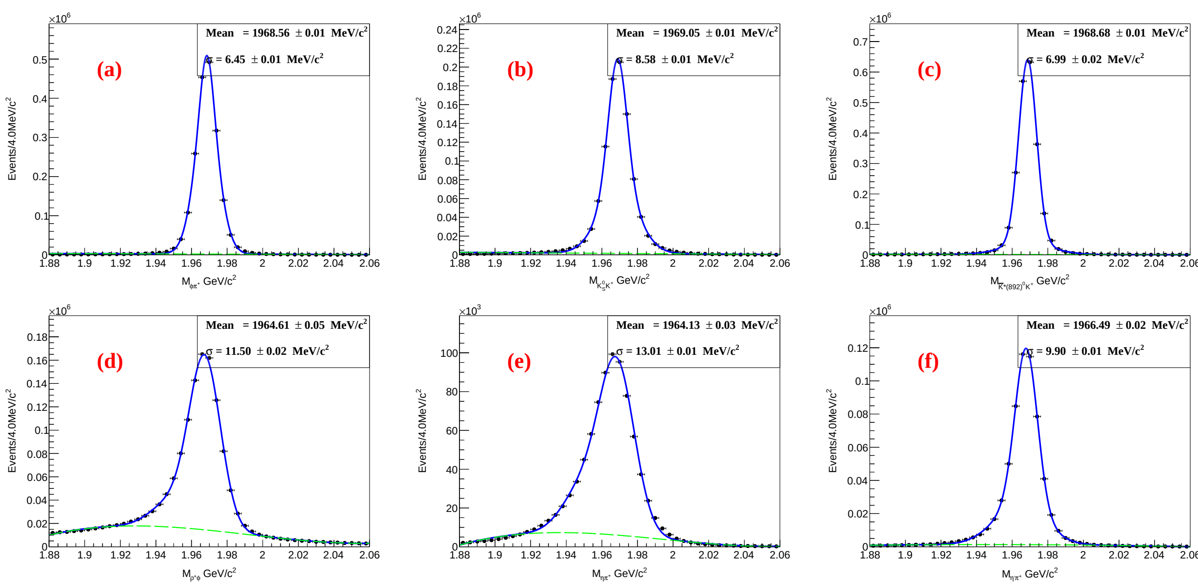

FIG. 13. The invariant mass distributions of the (a)$\phi\pi^+$, (b)$K_S^0K^+$, (c)$K^*(892)^0K^+$, (d)$\phi\rho^+$, (e)$\eta\pi^+$, (f)$\eta'\pi^+$ in the continuuum MC simulations, respectively. The curves show the best fit results using Gaussian functions for the D_s^+ signals.

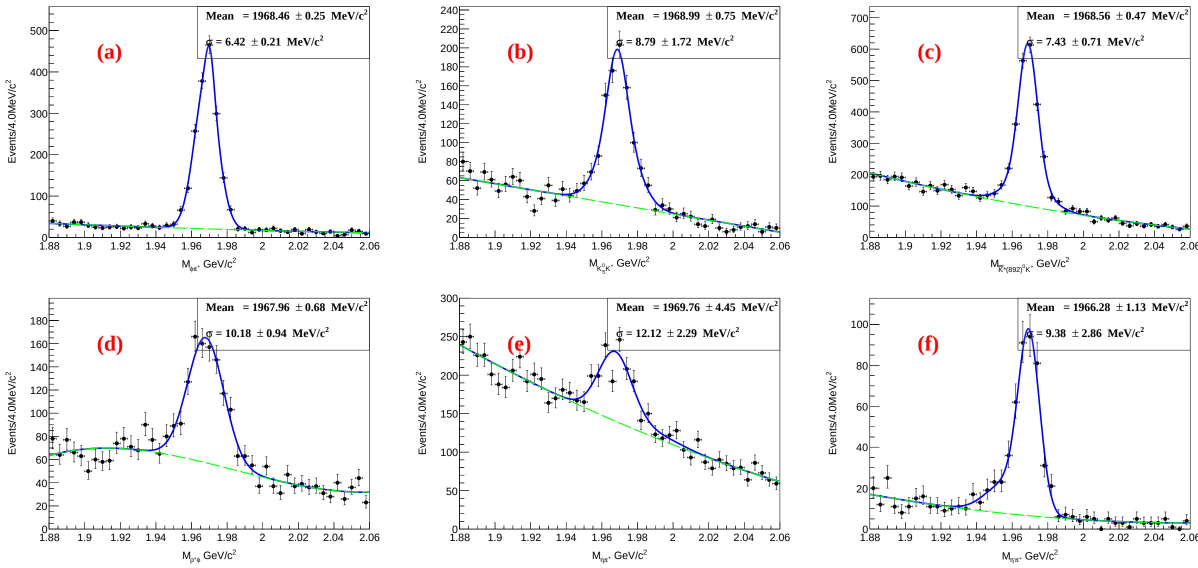

FIG. 14. The invariant mass distributions of the (a)$\phi\pi^+$, (b)$K_S^0K^+$, (c)$K^*(892)^0K^+$, (d)$\phi\rho^+$, (e)$\eta\pi^+$, (f)$\eta'\pi^+$ in the continuum data samples, respectively. The curves show the best fit results using Gaussian functions for the D_s^+ signals.

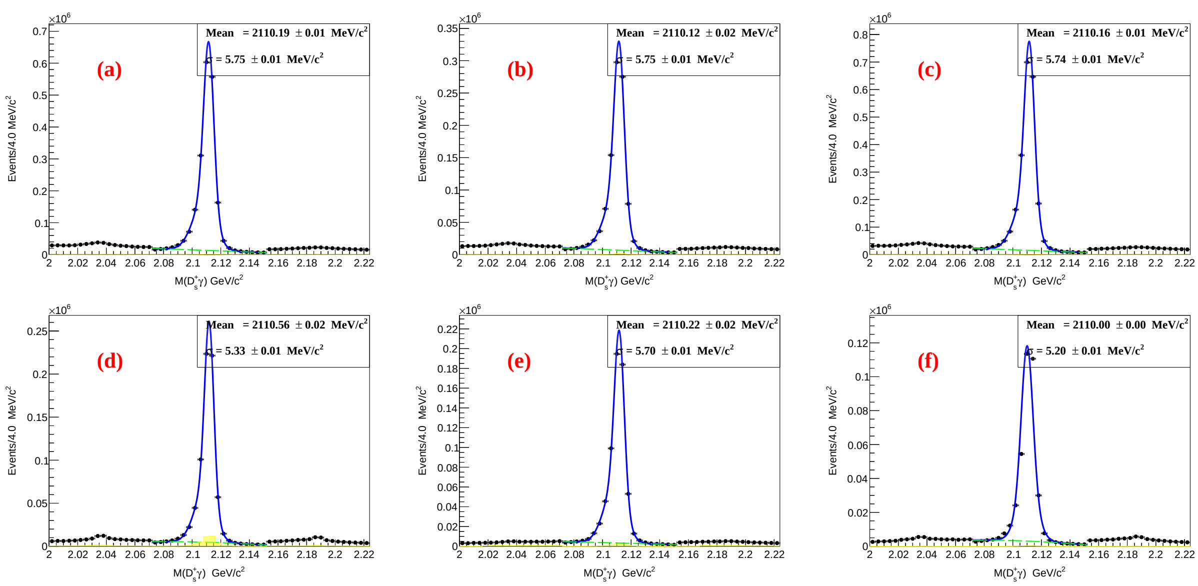

FIG. 15. The invariant mass distributions of D_s^{*+} candidates in mode $D_s^+ \to$ (a)$\phi\pi^+$, (b)$K_S^0K^+$, (c)$K^*(892)^0K^+$, (d)$\phi\rho^+$, (e)$\eta\pi^+$, (f)$\eta'\pi^+$ in the $\Upsilon(2S)$ MC simulations, respectively. The shaded histograms show the backgrounds estimated from the normalized D_s^+ mass sidebands. The curves show the best fit results using Gaussian functions for the D_s^{*+} signals.

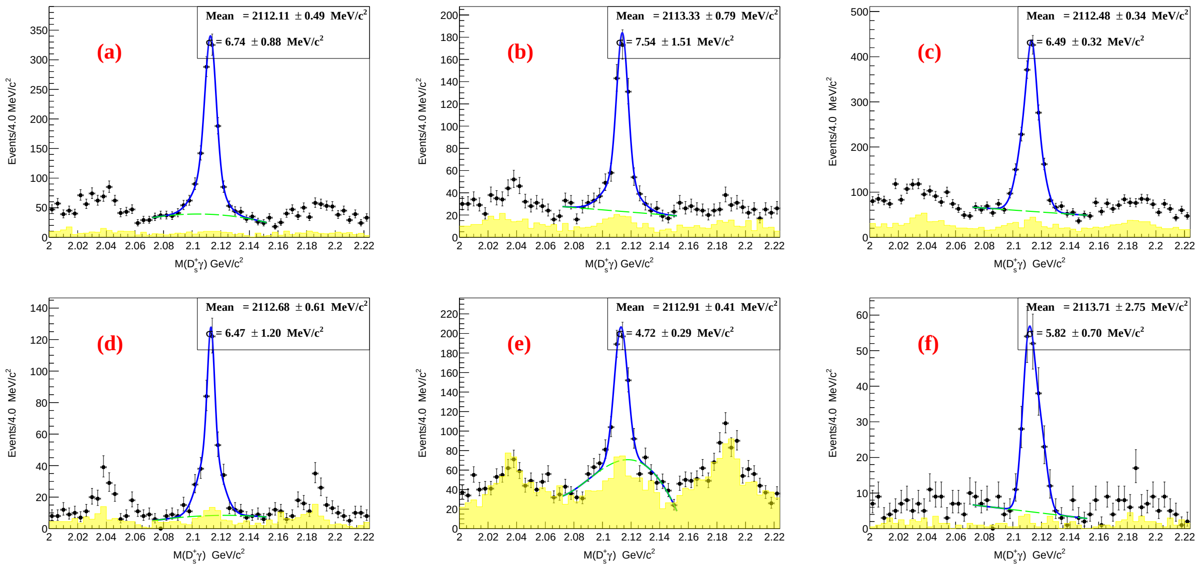

FIG. 16. The invariant mass distributions of D_s^{*+} candidates in mode $D_s^+ \to$ (a)$\phi\pi^+$, (b)$K_S^0K^+$, (c)$K^*(892)^0K^+$, (d)$\phi\rho^+$, (e)$\eta\pi^+$, (f)$\eta'\pi^+$ in the $\Upsilon(2S)$ data samples, respectively. The shaded histograms show the backgrounds estimated from the normalized D_s^+ mass sidebands. The curves show the best fit results using Gaussian functions for the D_s^{*+} signals.

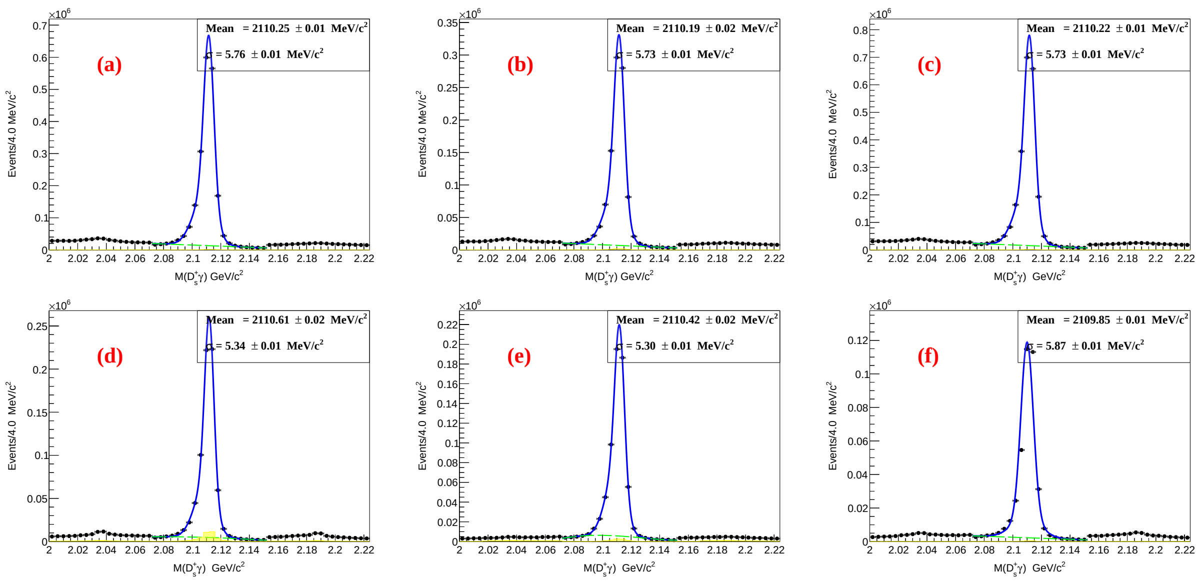

FIG. 17. The invariant mass distributions of D_s^{*+} candidates in mode $D_s^+ \to$ (a)$\phi\pi^+$, (b)$K_S^0K^+$, (c)$K^*(892)^0K^+$, (d)$\phi\rho^+$, (e)$\eta\pi^+$, (f)$\eta'\pi^+$ in the continuum MC simulations, respectively. The shaded histograms show the backgrounds estimated from the normalized D_s^+ mass sidebands. The curves show the best fit results using Gaussian functions for the D_s^{*+} signals.

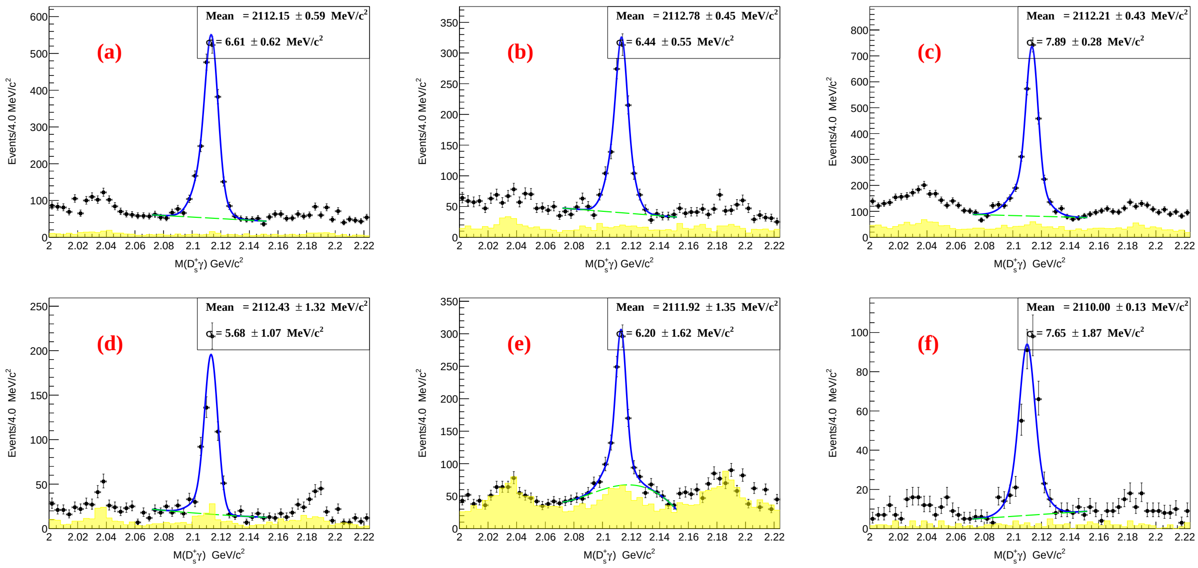

FIG. 18. The invariant mass distributions of D_s^{*+} candidates in mode $D_s^+ \to$ (a)$\phi\pi^+$, (b)$K_S^0 K^+$, (c)$K^*(892)^0 K^+$, (d)$\phi\rho^+$, (e)$\eta\pi^+$, (f)$\eta'\pi^+$ in the continuum data samples, respectively. The shaded histograms show the backgrounds estimated from the normalized D_s^+ mass sidebands. The curves show the best fit results using Gaussian functions for the D_s^{*+} signals.